NBSIR 83-2776

Determination of the Viscoelastic Shear Modulus Using Forced Torsional Vibrations

Center for Manufacturing Engineering
Automated Production Technology Division
U.S. Department of Commerce
National Bureau of Standards
Washington, D.C. 20234

Final Report

September 1983

NBSIR 83-2776

DETERMINATION OF THE VISCOELASTIC SHEAR MODULUS USING FORCED TORSIONAL VIBRATIONS

Edward B. Magrab

Center for Manufacturing Engineering
Automated Production Technology Division
U.S. Department of Commerce
National Bureau of Standards
Washington, D.C. 20234

Final Report

September 1983

U.S. DEPARTMENT OF COMMERCE, Malcolm Baldrige, *Secretary*
NATIONAL BUREAU OF STANDARDS, Ernest Ambler, *Director*

TABLE OF CONTENTS

FIGURE TITLES

ABSTRACT

A forced torsional vibration system has been developed to measure the shear storage and loss moduli on right circular cylindrical specimens whose diameter can vary from 2 to 9 cm and whose length can vary from 2 to 15 cm. The method and apparatus are usable over a frequency range of 80 to 550 Hz and a temperature range of -20°C to 80°C.

INTRODUCTION

Many methods exist for the experimental determination of the viscoelastic properties of materials. Some of these methods have been summarized in References 1 and 2 and those used more recently in a collection of abstracts in Reference 3. The present method described herein, which uses forced torsional vibrations, is an updated version of previous works (4,5). It was selected because it most easily met the requirements placed on the sample's geometry and dimensions, which was a circular cylinder whose diameter ranged from 2 to 9 cm and whose length ranged to 15 cm. This wide range of sizes is a consequence of the desire to use the same sample that was previously subjected to a different kind of material properties' test over a different (higher) frequency range. The method and apparatus described subsequently is usable over the frequency range from 50 - 550 Hz and a temperature range from - 20° to 80° C.

THEORY

Consider the forced harmonic torsional vibrations of a right circular cylinder having a frequency dependent complex viscoelastic shear modulus $G^*(f) = G'(f) + jG''(f)$, where $G'(f)$ is the shear storage modulus, $G''(f)$ the loss modulus and f the frequency. If a mass with mass moment of inertia J and a torsional spring of constant k are attached to one end of the cylinder as shown in Figure 1 and the other end of the cylinder is subjected to a harmonically varying torque, then the expression for the angular acceleration response ratio of the top plane of the cylinder to the bottom plane is given by (4,5)

$$A_o = \frac{(Acc)_{TOP}}{(Acc)_{BOT}} = \frac{r_t}{r_b} \left[C_1 \Omega^* \sin(\Omega^*) + \cos(\Omega^*) \right]^{-1} \qquad (1)$$

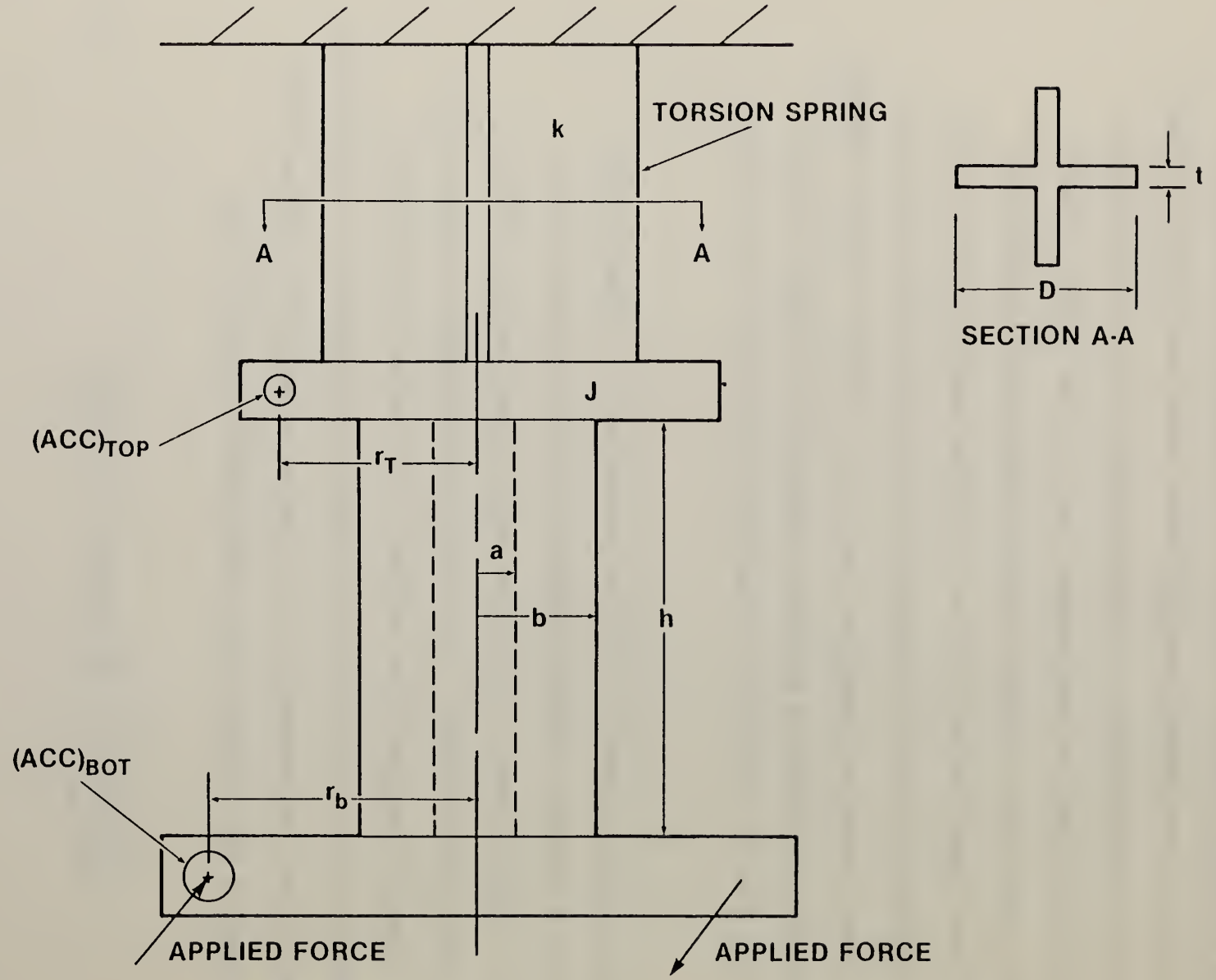

FIGURE 1 GEOMETRIC DESCRIPTION OF TORSION SPECIMEN AND ATTACHED SPRING AND MASS.

where

$$C_1 = \frac{2J[(f_m/f)^2 - 1]}{\pi\rho h(b^4 - a^4)} \tag{2}$$

$$\Omega^* = x - jy$$

$$f_m = \frac{1}{2\pi}\sqrt{\frac{k}{J}}$$

$$x = 2\pi\sqrt{\frac{\rho f^2 h^2}{p}}\cos(\theta/2)$$

$$y = 2\pi\sqrt{\frac{\rho f^2 h^2}{p}}\sin(\theta/2) \tag{3}$$

$$p = \left[G'^2 + G''^2\right] 1/2$$

$$\theta = \tan^{-1}(G''/G') \tag{4}$$

and ρ is the density of the cylinder, h its length, b its outer radius, a its inner radius and G"/G' the loss tangent. The quantity f_m is the natural frequency of the attached spring-mass system with the cylindrical specimen removed. The quantity r_t is the distance from the center of the axis of the cylinder to the center of the top accelerometer and r_b is the distance from the axis to the point of application of the applied force, which coincides with the location of the bottom accelerometer.

Substituting Eq. (3) into Eq. (1) yields

$$A_o = R\, e^{j\phi} \tag{5}$$

where

$$R = \left(\frac{r_t}{r_b}\right)(A^2 + B^2)^{-1/2}$$

$$\phi = \tan^{-1}(B/A) \tag{6}$$

and

$$A = [C_1 x\sin(x) + \cos(x)]\cosh(y) - C_1 y\cos(x)\sinh(y)$$

$$B = [C_1 x\cos(x) - \sin(x)]\sinh(y) + C_1 y\sin(x)\cosh(y) \tag{7}$$

Thus, if R and ϕ are the measured amplitude ratio and phase angle, respectively, and all the physical and geometric parameters of the specimen are determined by other means, then G' and G" can be found using Eqs. (6) and (7). However, because of the complexity of these equations, G' and G" cannot be solved for explicity. The numerical procedure used to obtain these quantities is described in Appendix I.

As the excitation frequency approaches zero and $f \ll f_m$ Eq. (1) becomes

$$A_o = \left(\frac{r_t}{r_b}\right)\left[1 + \frac{C_o}{G}\right]^{-1} \tag{8}$$

where

$$C_o = \left(\frac{8\pi h}{b^4 - a^4}\right) J f_m^2 \tag{9}$$

and G is a nominal value for p. The range of values for C_o, in N/m^2, for the experimental setup are approximately $2.5 \times 10^5 \leq C_o \leq 2 \times 10^8$. Thus for materials with a shear modulus of 3×10^7 N/m^2, A_o will vary from a value slightly less than r_t/r_b to a value of approximately $(r_t/r_b)/8$.

DESIGN CONSIDERATIONS

1. General Requirements

The general requirements are that (1) the specimens can range in size to approximately 15 cm in length and 9 cm in diameter; (2) the shear moduli can be as low as 3×10^6 N/m^2; (3) the method provides the shear modulus over a broad frequency range from 50 to 550 Hz and temperature range from -20° to 80 °C.

2. Temperature Considerations

The temperature requirements place a limit on the overall size of the test fixture, for it has to fit into a temperature chamber of reasonable size. It also has to weigh a modest amount so that one could place it into a chamber without the chamber requiring additional structural support. Lastly, in order to operate the vibration exciters over the temperature range, the exciters have to be air cooled/heated with room temperature air (20 °C) so that the springs that sustain the exciter's moving element retain their desired properties.

The temperature of the specimen is determined from the placement of a thermocouple on the specimen's surface and is read by a digital output device with an accuracy of ± 1 °C.

3. Fixture

According to the theory used to determine the shear modulus from the experimentally determined data, the specimen should be subjected to torsional motion only, with no bending of the specimen. In addition, the fixture itself must be free from structural resonances over a broad frequency range and for test samples of varying length and diameter. The design chosen was a combination of certain features of previous works [4, 5] and is shown in Figure 2.

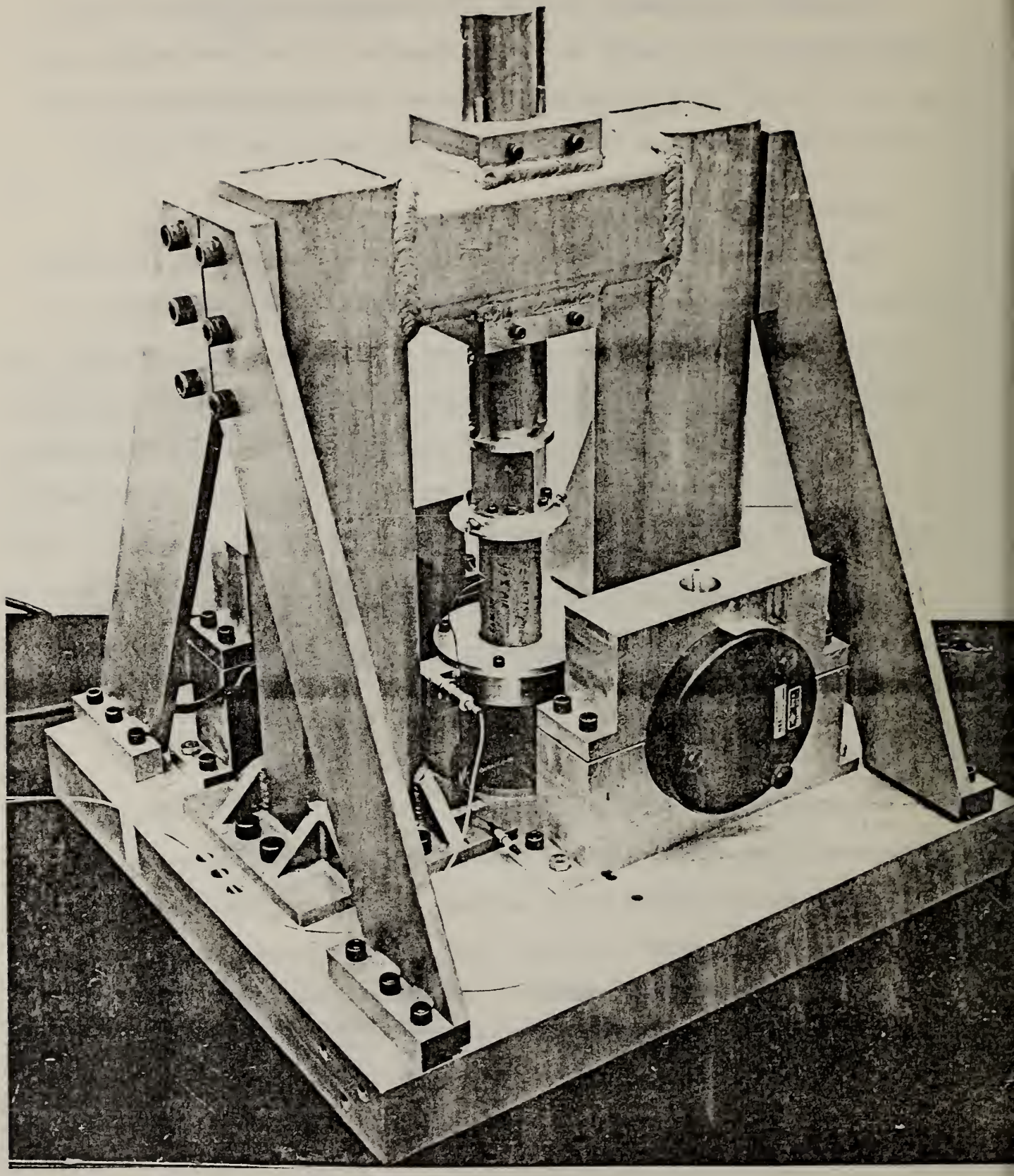

FIGURE 2 FORCED TORSIONAL VIBRATION APPARATUS.

To minimize bending the top and bottom torsional springs have an "x" cross-section, which is very stiff in bending compared to its twisting resistance. To show this consider a single force F acting on the spring through a moment arm about the center of the spring of radius r_b. The displacement due to bending, s_B, is

$$s_B = \frac{1}{3}\frac{FL^3}{EI}$$

and that due to rotation

$$s_T = \frac{Fr_b^2 L}{KG}$$

where G and E are the shear and tensile moduli of the spring, respectively, L is its length and I and K are the moment of inertia and the torsion constant of the cross-section, respectively. The accelerations of the spring are proportional to these displacements. Thus a good measure of their relative resistance to this unbalanced torque is their ratio. Hence,

$$\frac{s_B}{s_T} = \frac{1}{6(1+\nu)}\left(\frac{L}{r_b}\right)^2 \frac{K}{I}$$

where ν is Poisson's ratio. For the "x" cross-section shown in Figure 1,

$$K \cong \frac{2}{3} Dt^3$$

$$I \cong \frac{tD^3}{12} \qquad (10)$$

Therefore,

$$\frac{s_B}{s_t} = \left(\frac{L}{r_b}\right)^2 \left(\frac{t}{D}\right)^2 \tag{11}$$

The bottom spring has the following dimensions: L = 8.26 cm, r_b = 7.46 cm, t = 0.32 cm and D = 10.16 cm. Using these values in Eq. (11) yields that $s_B/s_T \cong 0.001$. Thus, the bending displacements can be expected to be on the order of a thousand times less than the desired torsionally induced displacements. In the actual system two dynamic exciters are used, which eliminates most of the unbalanced force. The output force of the shakers, however, is not controlled, and it is assumed that the same input voltage to both exciters yields approximately the same output force. However, because of this great difference in stiffnesses, any small imbalance does not strongly couple to the system. For the top spring the parameters in Eq. (10) are: L $\cong$ 5.08 cm, t = 0.0794 cm and D = 6.99 cm. Equation (10) now yields $s_B/s_T \cong 0.0002$.

The experimental confirmation of the excitation portion of the fixture's resistance to bending is shown in Figure 3. The input signal to the shakers was broadband random noise. A commercial digital frequency analyzer was used to obtain the time-averaged transfer function of the input voltage to the shakers to the bottom accelerometer. The result is shown in Figure 3. The absence of any resonance peaks until approximately 680 Hz, except the one directly related to the first torsional resonance of spring-mass system, can be seen. This indicates that the useful frequency range of the fixture is as high as approximately 550 Hz. The torsional natural frequency of the bottom spring mass system is of no consequence in the experiment because the magnitude of the input acceleration is kept relatively constant over the entire test frequency range.

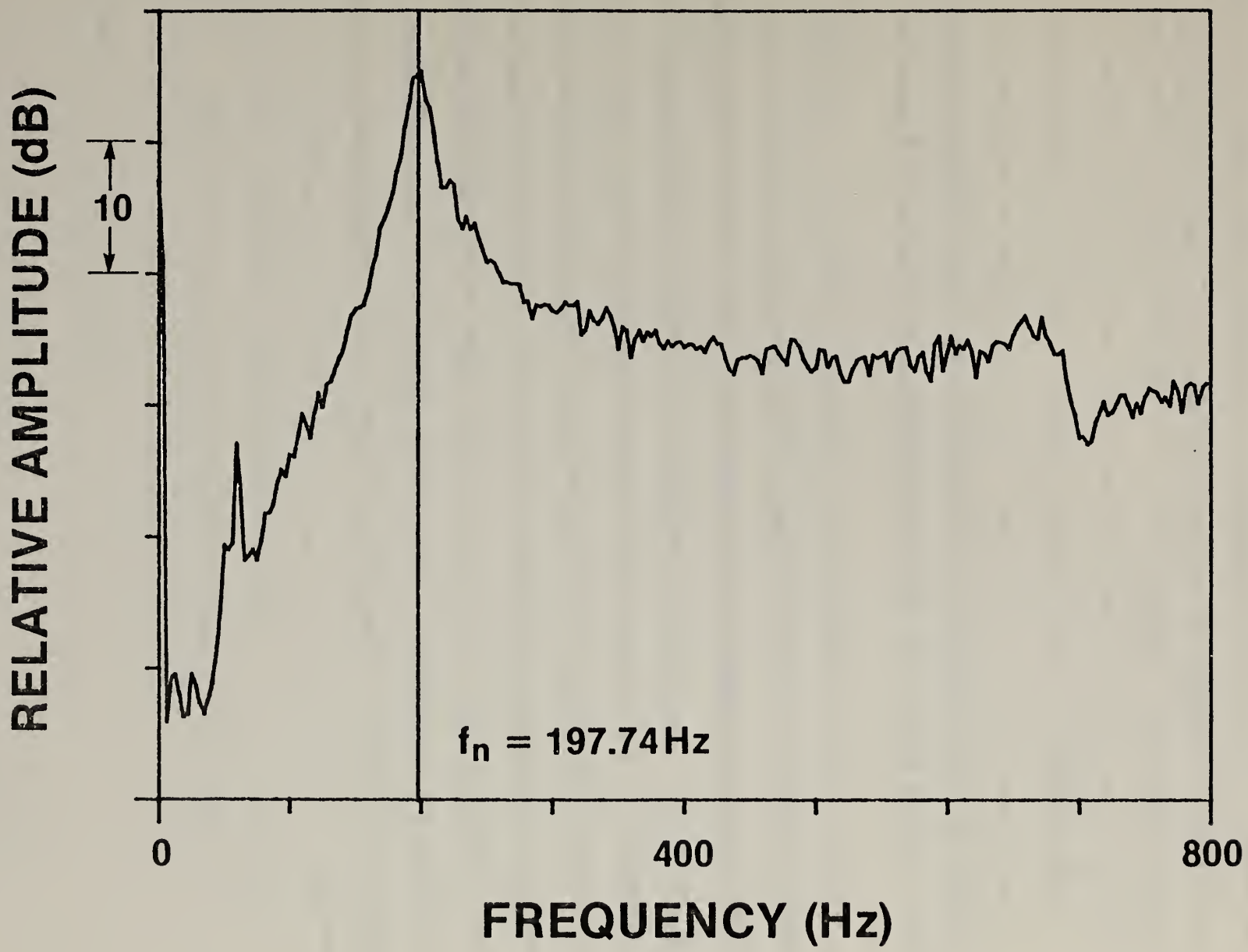

FIGURE 3 TRANSFER FUNCTION OF BOTTOM TORSIONAL SPRING AND ATTACHED MASS.

4. Determination of J and f_m

The top end of the top torsion spring is bolted to a movable solid steel cylinder as shown in Figure 2. According to the theory developed previously, this connection must be rigid compared to the torsion spring itself. The ratio of the torsional rigidity of the solid cylinder, K_c, to that of the torsion spring, K (given by Eq. (10)), is

$$\frac{K_c}{K} = \frac{3\pi}{64}\left(\frac{D}{t}\right)^3$$

Substituting in the appropriate dimensional values for the fixture shown in Figure 2 yields $K_c/K \cong 10^5$. Thus, the assumption of rigidity is a good one.

Another important consideration is the range of values for J, the mass moment of inertia of the attached mass. For a given natural frequency of this system the specimen, when connected to J, must be able to influence both the value of f_m and, more importantly, its damping. An indication of the magnitude of the parameters that influence these properties can be approximately determined by assuming that the vibrating system consists of the inertia J connected to two springs; one is the "tee" cross-section torsion spring already discussed and the other is the spring formed by the torsional resistance of the specimen, assuming that its internal damping can be ignored in this portion of the analysis. The natural frequency of this new system, f_m', is then given by

$$f_m' = f_m[1 + C_2]^{1/2} \tag{12}$$

where f_m is given by Eq. (3) and

$$C_2 = \frac{\pi}{2}\left(\frac{G}{h}\right)\frac{(b^4-a^4)}{(2\pi f_m)^2}\left(\frac{1}{J}\right) \tag{13}$$

It is seen that in order for C_2 to be greater than one, the combination of h, f_m and J must be chosen carefully for a given material. Unfortunately the class of materials that are to be tested are very weak in torsion and typically have a shear modulus of 4 to 15 x 10^6 N/m^2. Consequently the design requires that J, h, and f_m be as small as possible. There are, of course, some physical limitations in just how small J can be made. In the apparatus shown in Figure 2, J = 1.8972 $kg\text{-}cm^2$. The computational procedure to obtain J is given in Appendix II.

Whereas J was computed, the natural frequency of the attached spring/mass system, f_m, without the test specimen attached was determined experimentally by using a digital frequency analyzer in its transfer function mode. The excitation was applied with a hammer to one of the "ears" (see Figs. 2 and A-2) of the top mass. The noncontacting end of the hammer had an accelerometer mounted to it. The resulting motion of the spring/mass was recorded by the accelerometer mounted on one of the "ears." Using the zoom capability of the analyzer, f_m was determined to within $\pm$0.25 Hz, which, for natural frequencies $f_m > 100$ Hz results in an uncertainty of 0.25% or less. The results for two torsion springs, one with t = 0.7938 mm and the other t = 1.588 mm (see Figure 1) and for two thickness of the accelerometer mounting disk (see Figure A-2) are summarized in Table 1. From the discussion in the preceding paragraph it is seen that for the weaker class of materials the spring/mass combinations resulting in the lower set of f_m should be used.

Table 1

Values of f_m for Four Combinations of Springs and Inertias (J)

	f_m(Hz)	
Spring flange thickness (mm)	J = 1.8972 kg-cm^2 (h_A= 6.35 mm)	J = 2.3652 kg-cm^2 (h_A= 12.75 mm)
0.7938	100.75	89.00
1.588	283.00	255.00

5. Specimen Mounting

In order that the specimen be mounted concentrically with respect to the top and bottom springs and to eliminate any pre-twist of the specimen, the following technique was employed. Two discs, one 12.3 cm in diameter that attaches to the bottom "ears" and the other, 6.9 cm in diameter that attaches to the top "ears" and which is included in the calculation of J, each have on one of its faces a concentric raised disk 1.5 mm high and 12.7 mm in diameter. These disks are mounted on their respective bell cranks with these raised disks facing each other. Prior to mounting the cylindrical specimen, the specimen is placed in a lathe to have each of its end planes turned smooth and perpendicular to its axis. In addition, a concentric cylindrical depression is turned on each of the end planes that is 1.59 mm deep and 12.7 mm in diameter. Epoxy is applied to each end plane of the cylindrical specimen and the specimen is placed onto the bottom disk. The top spring mass assembly is then lowered onto the top of the specimen and the epoxy is allowed to cure.

INSTRUMENTATION

The instrumentation system used to measure the accelerometers' amplitude ratio and phase angle is shown in Figure 4. The electrodynamic vibration exciters are connected in parallel and receive their input voltage from an amplifier with the capacity to provide 15A rms into 1 ohm. The input to the amplifier is connected to an oscillator. The exciters themselves have an impedance of approximately 2 ohms and require 5A rms to obtain their rated output force. The oscillator's output voltage amplitude and frequency are under computer control.

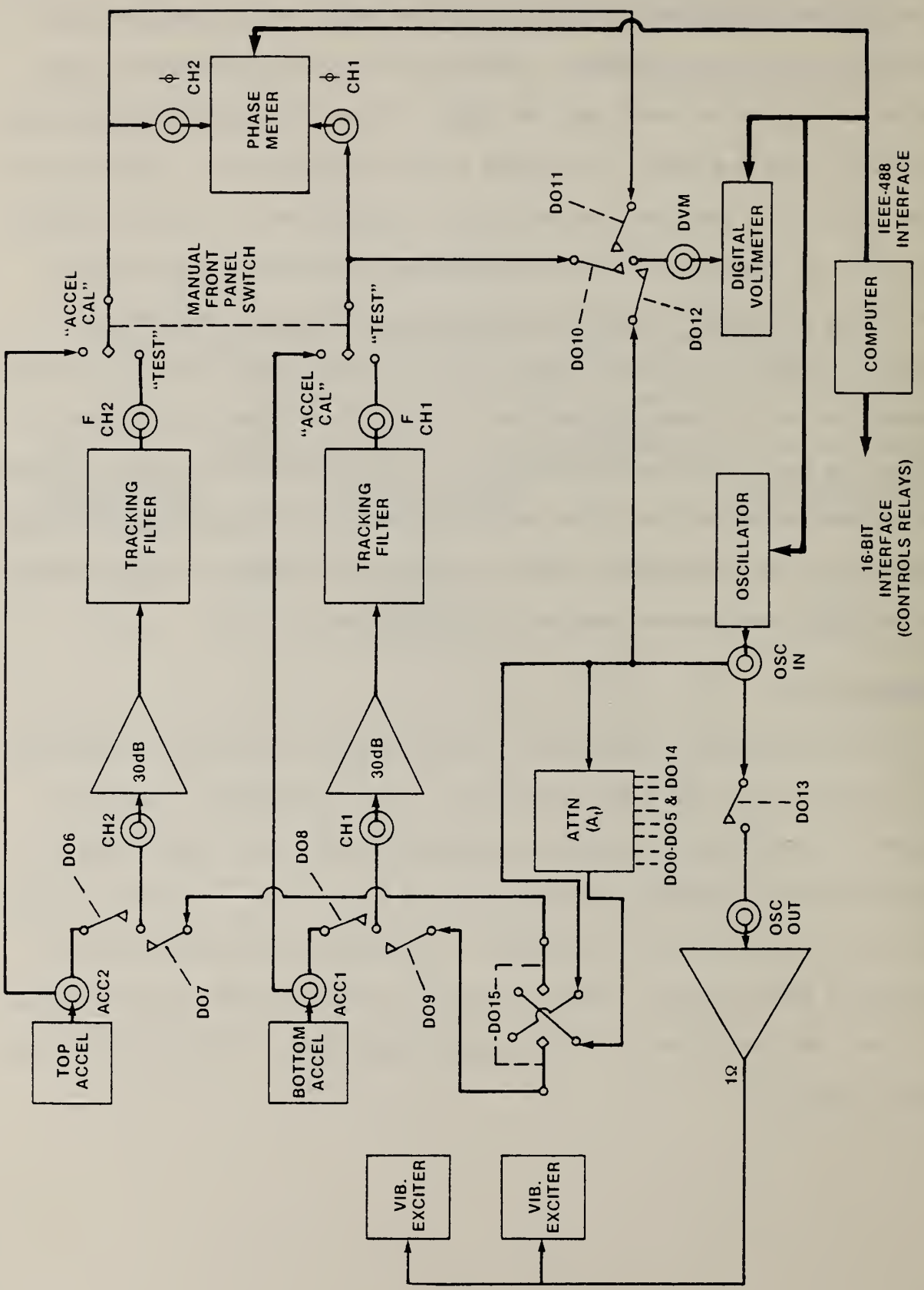

FIGURE 4 SCHEMATIC OF COMPLETE INSTRUMENTATION SYSTEM.

The accelerometers have a sensitivity of nominally 10 mV/g and have a unity gain preamplifier built into them. The output signals from the accelerometers are then amplified 30 dB and passed through two 2 Hz bandwidth tracking filters. The tracking frequency is provided by a second output signal from the oscillator which remains constant at 1 V. This 1 V signal is amplified to meet the tracking filter's requirement of 3.5 V. The 30 dB gain given to each accelerometer signal provides better use of the dynamic range of the tracking filters and uses the digital phasemeter in a voltage range in which its accuracy is better, namely, at levels above 50 mV rms. To maintain control over the voltage levels throughout the electronic measuring system, the output voltage of the oscillator is continuously adjusted so that the output voltage of the bottom accelerometer remains approximately constant at 2.5 mV rms over the entire test frequency range.

The signals from the output of the tracking filters are sent directly to the digital phasemeter and the digital voltmeter, both of which are under computer control. However, the signals to the voltmeter are read sequentially with the aid of a computer controlled switching setup described in detail in Appendix III. The phasemeter has an autocalibration feature which is employed every sixth measurement to insure that the phase measurements are as precise as possible. The digital voltmeter is used in its autoranging mode, since the output voltage for the upper accelerometer differs widely over the frequency range.

The purpose for the attenuator (labeled ATTN) is discussed in detail subsequently.

To accurately measure the acceleration ratio of the top accelerometer to the bottom one and the phase angle between them, one must remove from the measured data the influences of any electronics inserted between the electrical

signal at the output of the accelerometers and the recording instruments: the digital voltmeter and the digital phasemeter. The ultimate accuracy of the measurement depends, of course, on the accuracy of the voltmeter and the phasemeter. In this experiment the voltmeter has an accuracy of approximately $\pm$0.2 dB for rms voltage above 100 mV and $\pm$0.3 dB for voltages less than 100 mV and greater than 100 μV over the frequency range 1 to 2000 Hz. The phasemeter has an accuracy of $\pm$0.1° for rms voltages greater than 50 mV and $\pm$0.2° for rms voltages as low as 1 mV from 50 Hz to 50 KHz.

The effects of the intervening electronics are removed in the following manner. Consider the simplified equipment diagram given in Figure 5. Let $H_j(f)$ be the transfer function of the accelerometer's built-in impedance converters, H_{Gj} the transfer function of the 30 dB fixed gain amplifiers, and H_{Fj} the transfer function of the tracking filter, where j = 1 refers to the bottom accelerometer channel and j = 2 to the top channel. The true output signal from the accelerometers, V_j, are related to the signals appearing at the inputs to the digital voltmeter and phasemeter, V_{Rj}, as follows:

$$V_{Rj} = V_j H_j H_{Gj} H_{Fj}, \quad j=1,2 \tag{14}$$

Solving Eq. (14) for the acceleration ratio $A_o = V_2/V_1$ yields

$$\frac{V_2}{V_1} = \left(\frac{V_{R2}}{V_{R1}}\right)\left(\frac{1}{C}\right) \tag{15}$$

where C is a complex quantity given by

$$C = \left(\frac{H_2}{H_1}\right)\left(\frac{H_{G2}H_{F2}}{H_{G1}H_{F1}}\right) \tag{16}$$

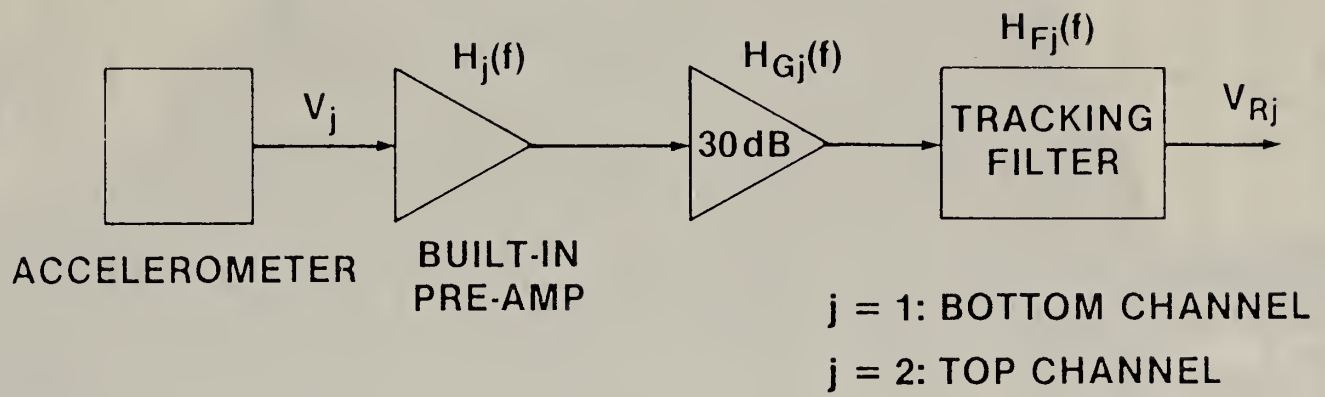

FIGURE 5 SIMPLIFIED VERSION OF A PORTION OF THE INSTRUMENTATION SYSTEM.

Thus, the amplitude ratio and phase angle are, respectively,

$$\left|\frac{V_2}{V_1}\right| = \left|\frac{V_{R2}}{V_{R1}}\right| \left|\frac{1}{C}\right|$$

$$\phi_{21} = \phi_{R21} - \phi_c \tag{17}$$

where $|V_{R2}/V_{R1}|$ is the ratio of the values read from the digital voltmeter and ϕ_{R21} is the value read from the digital phasemeter. The quantity $|C^{-1}|$ is the correction that must be isolated and measured in order to remove the influence of the electronic components on the amplitude measurement and ϕ_c is the quantity that must be isolated and measured to remove the influence on the phase angle measurement.

To remove the effects of C at a given temperature, we proceed by first removing H_{Gj} and H_{Fj} from the measurement chain and perform a back-to-back calibration of the two accelerometers. Thus, $V_2 = V_1 e^{j\pi}$ (since one accelerometer is upside down with respect to the other) and

$$\left|\frac{H_2}{H_1}\right| = \left|\frac{V_{R2}}{V_{R1}}\right|_{B-B}$$

$$\phi_{21} = \phi_{BB} + \pi \tag{18}$$

where $|V_{R2}/V_{R1}|$ is determined directly from the reading of the digital voltmeter and ϕ_{B-B} directly from the digital phasemeter. A picture of the back-to-back calibration fixture is shown in Figure 6.

We now disconnect the accelerometers from the measurement chain and replace them by two signals at the same frequency that differ only in amplitude and not phase. Thus $V_1H_1 = V_I$ and $V_2H_2 = A_tV_I$ where V_I is the amplitude of the input voltage to both channels and $0 < A_t < 1$. The attenuation A_t is introduced because of the

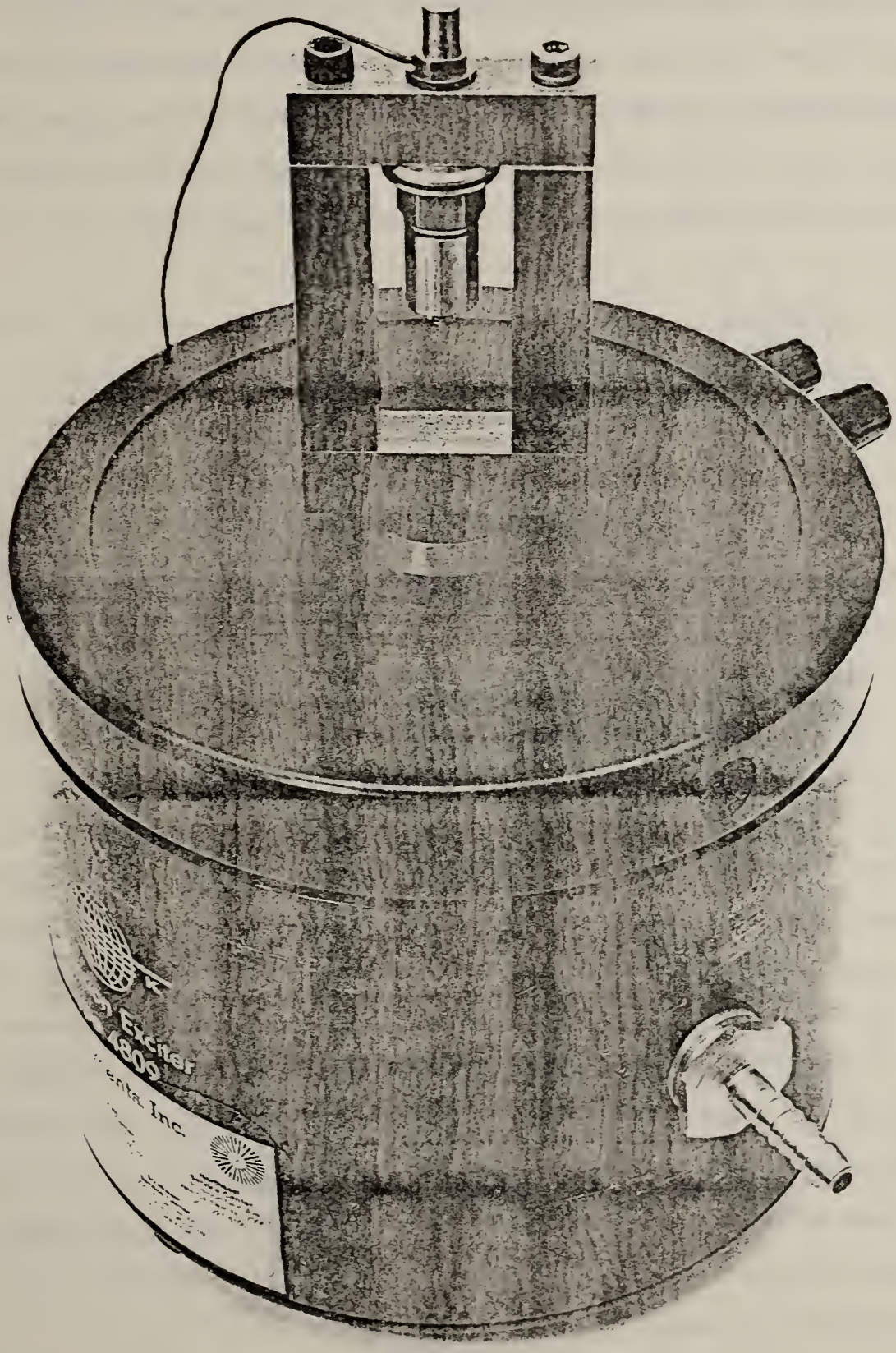

FIGURE 6 BACK-TO-BACK CALIBRATION FIXTURE.

high degree of amplitude and phase nonlinearity of the tracking filters. The introduction of the attenuator allows the input signals to each channel to be approximately equal (to within ± 2.5 dB) to each accelerometer's output signal. In the actual test procedure the attenuator A_t can be introduced to either channel depending on whether or not the accelerometer's output signal ratio is greater than or less than 1. If the A_t is switched, then A_t is simply replaced by $1/A_t$ in the subsequent results. Equation (17) then yields

$$\left|\frac{H_{G2}H_{F2}}{H_{G1}H_{F1}}\right| = A_t \left|\frac{V_{R2}}{V_{R1}}\right|_I$$

$$\phi_{21} = \phi_I \tag{19}$$

where $|V_{R2}/V_{R1}|_I$ is determined directly from the readings of the digital voltmeter and ϕ_I directly from the digital phasemeter. Using Eqs. (18) and (19) yields the desired result

$$\left|\frac{V_2}{V_1}\right| = \left|\frac{V_{R2}}{V_{R1}}\right| \left[A_t \left|\frac{V_{R2}}{V_{R1}}\right|_{B-B} \left|\frac{V_{R2}}{V_{R1}}\right|_I\right]^{-1}$$

$$\phi_{21} = \phi_{R21} - \phi_{BB} - \pi - \phi_I \tag{20}$$

The test procedures used to determine the quantities in Eq. (20) are done under computer control using a set of 16 relays. The details of this switching system are given in Appendix III.

In the actual testing of the accelerometer's back-to-back response it was found that at a given temperature it could be assumed that the accelerometers' relative amplitudes are constant over the frequency range of interest and that the phase difference was essentially zero. In other words $|V_{R2}/V_{R1}|_{BB} = C_3$, a constant and $\phi_{BB} = 0$ in Eq. (18). The constant C_3 is determined at each temperature at a nominal frequency of 200 Hz.

The errors associated with the measurement of the amplitude ratio and phase angle cannot be easily related to the resulting errors in the determination of the shear modulus because of the highly nonlinear nature of Eqs. (5) to (7). Consequently, to get an estimate of the accuracy of the numerically evaluated G' and G", the following procedure is used. Equation (1) is evaluated over a frequency range for an assumed value of G' and G". This results in a set of amplitude ratios (A_o) and phase angles (ϕ) as a function of frequency. The set of A_o and ϕ are then altered by the accuracy of the digital voltmeter and phasemeter, and the inverse problem is considered. Thus, at a given frequency we change the amplitude ratios by up to ± 0.2 dB and the phase angle by up to $\pm 0.3°$ and solve Eq. (11) for G' and G". The results are shown in Tables 2 and 3 for $J = 1.9$ kg-cm^2, $f_m = 100$ Hz, $\rho = 1000$ kg/m^3, $G' = 20 \times 10^6$ N/m^2, $G"/G' = 0.4$, $h = 10$ cm, $b = 5$ cm and $a = 0$. Since the technique only works in the region of the systems resonance, frequencies above 175 Hz were not considered.

It is seen from the results presented in Tables 2 and 3 that the percentage errors in G' and G"/G' are asymmetrical with respect to the errors in the amplitude and phase at frequencies away from f_m and large and unequal at frequencies at or near f_m, with the largest errors occuring in the loss tangent.

Another inaccuracy in the determination of the values for G' and G" are errors due to the calculation of J and the determination of f_m in Eq. (2). Using a procedure similar to what was done above gives the effects of J and f_m shown in Table 4. There are no effects of the errors in J and f_m on the ratio G"/G'. Thus, the results in Table 4 apply to both G' and G", individually. The total error in the determination of G' and G" are the sum of the errors appearing in Tables 2 and 4, and 3 and 4.

TABLE 2

PERCENTAGE DIFFERENCES IN COMPUTED STORAGE MODULUS
AS FUNCTION OF ERRORS IN AMPLITUDE AND PHASE

	50 Hz					75 Hz				
PHASE ERROR (Deg.)	AMPLITUDE RATIO ERROR (dB) -.2	-.1	0.0	.1	.2	-.2	-.1	0.0	.1	.2
-.3	5.6	2.3	-1.2	-4.8	-8.6	9.4	3.9	-2.2	-8.8	-16.2
-.2	5.9	2.6	-.8	-4.4	-8.2	9.9	4.5	-1.5	-8.0	-15.2
-.1	6.2	3.0	-.4	-4.0	-7.7	10.4	5.1	-.7	-7.1	-14.1
0.0	6.5	3.4	0.0	-3.5	-7.2	11.0	5.7	0.0	-6.2	-13.0
.1	6.9	3.7	.4	-3.1	-6.7	11.5	6.4	.7	-5.3	-12.0
.2	7.2	4.1	.8	-2.6	-6.3	12.0	7.0	1.5	-4.4	-10.9
.3	7.5	4.4	1.2	-2.2	-5.8	12.6	7.6	2.3	-3.5	-9.8

	100 Hz					125 Hz				
PHASE ERROR (Deg.)	AMPLITUDE RATIO ERROR (dB) -.2	-.1	0.0	.1	.2	-.2	-.1	0.0	.1	.2
-.3	-12.1	-3.8	4.2	11.6	18.1	-1.2	-.3	.7	1.6	2.5
-.2	-14.8	-5.8	2.8	10.5	17.3	-1.4	-.5	.4	1.4	2.3
-.1	-17.5	-7.7	1.4	9.5	16.5	-1.7	-.7	.2	1.2	2.1
0.0	-20.2	-9.6	0.0	8.4	15.7	-1.9	-1.0	0.0	.9	1.9
.1	-22.9	-11.5	-1.4	7.4	15.0	-2.2	-1.2	-.2	.7	1.7
.2	-25.6	-13.4	-2.7	6.5	14.3	-2.4	-1.4	-.4	.5	1.5
.3	-28.3	-15.2	-4.0	5.5	13.6	-2.7	-1.7	-.7	.3	1.3

	150 Hz					175 Hz				
PHASE ERROR (Deg.)	AMPLITUDE RATIO ERROR (dB) -.2	-.1	0.0	.1	.2	-.2	-.1	0.0	.1	.2
-.3	.4	.3	.2	.2	.1	1.1	.6	.1	-.4	-.9
-.2	.3	.3	.2	.1	.0	1.1	.6	.1	-.4	-.9
-.1	.3	.2	.1	.0	-.1	1.0	.5	.0	-.5	-1.0
0.0	.2	.1	0.0	-.1	-.2	1.0	.5	0.0	-.5	-1.0
.1	.1	.0	-.1	-.2	-.2	1.0	.5	-.0	-.5	-1.0
.2	.0	-.1	-.2	-.2	-.3	.9	.4	-.1	-.6	-1.0
.3	-.1	-.2	-.2	-.3	-.4	.9	.4	-.1	-.6	-1.1

TABLE 3

PERCENTAGE DIFFERENCES IN COMPUTED LOSS TANGENT
AS FUNCTION OF ERRORS IN AMPLITUDE AND PHASE

	50 Hz					75 Hz				
PHASE ERROR (Deg.)	AMPLITUDE RATIO ERROR (dB)					AMPLITUDE RATIO ERROR (dB)				
	-.2	-.1	0.0	.1	.2	-.2	-.1	0.0	.1	.2
-.3	10.5	7.9	5.1	2.1	-1.2	19.0	14.3	9.0	2.9	-4.2
-.2	8.9	6.2	3.4	.3	-3.0	16.3	11.5	6.0	-.3	-7.7
-.1	7.3	4.6	1.7	-1.4	-4.8	13.7	8.7	3.0	-3.5	-11.1
0.0	5.7	3.0	0.0	-3.2	-6.6	11.0	5.9	0.0	-6.7	-14.6
.1	4.1	1.3	-1.7	-4.9	-8.4	8.3	3.0	-3.0	-10.0	-18.0
.2	2.5	-.3	-3.4	-6.7	-10.3	5.6	.2	-6.0	-13.2	-21.5
.3	.9	-2.0	-5.1	-8.5	-12.1	3.0	-2.7	-9.1	-16.4	-25.0

	100 Hz					125 Hz				
PHASE ERROR (Deg.)	AMPLITUDE RATIO ERROR (dB)					AMPLITUDE RATIO ERROR (dB)				
	-.2	-.1	0.0	.1	.2	-.2	-.1	0.0	.1	.2
-.3	-56.2	-32.1	-14.3	-.7	10.2	-7.5	-4.6	-1.7	1.0	3.6
-.2	-49.8	-26.6	-9.6	3.5	13.9	-6.9	-4.0	-1.2	1.5	4.1
-.1	-43.3	-21.1	-4.8	7.8	17.7	-6.3	-3.4	-.6	2.1	4.7
0.0	-36.7	-15.6	0.0	12.0	21.4	-5.7	-2.8	0.0	2.7	5.2
.1	-30.2	-10.1	4.8	16.2	25.2	-5.1	-2.2	.6	3.2	5.8
.2	-23.7	-4.5	9.6	20.4	29.0	-4.5	-1.6	1.2	3.8	6.3
.3	-17.1	1.0	14.4	24.6	32.8	-3.8	-1.0	1.8	4.4	6.9

	150 Hz					175 Hz				
PHASE ERROR (Deg.)	AMPLITUDE RATIO ERROR (dB)					AMPLITUDE RATIO ERROR (dB)				
	-.2	-.1	0.0	.1	.2	-.2	-.1	0.0	.1	.2
-.3	-3.0	-1.6	-.1	1.3	2.7	-1.4	-.5	.5	1.4	2.4
-.2	-3.0	-1.5	-.1	1.3	2.7	-1.6	-.6	.3	1.3	2.2
-.1	-2.9	-1.5	-.0	1.4	2.8	-1.8	-.8	.2	1.1	2.1
0.0	-2.9	-1.4	0.0	1.4	2.8	-1.9	-1.0	0.0	1.0	1.9
.1	-2.8	-1.4	.1	1.5	2.9	-2.1	-1.1	-.2	.8	1.8
.2	-2.8	-1.3	.1	1.5	2.9	-2.3	-1.3	-.3	.6	1.6
.3	-2.7	-1.3	.2	1.6	3.0	-2.4	-1.4	-.5	.5	1.4

TABLE 4

PERCENTAGE DIFFERENCES IN COMPUTED STORAGE MODULUS
AS FUNCTION OF ERRORS IN J AND Fm

	50 Hz					75 Hz				
INERTIA ERROR (%)	NATURAL FREQUENCY ERROR (%)					NATURAL FREQUENCY ERROR (%)				
	-1.0	-.5	0.0	.5	1.0	-1.0	-.5	0.0	.5	1.0
-1.0	3.9	2.5	1.1	-.3	-1.8	7.1	4.2	1.3	-1.6	-4.6
-.5	3.3	1.9	.5	-.9	-2.3	6.5	3.6	.6	-2.3	-5.3
0.0	2.8	1.4	0.0	-1.4	-2.9	5.9	2.9	0.0	-3.0	-5.9
.5	2.3	.9	-.5	-2.0	-3.4	5.3	2.3	-.6	-3.6	-6.6
1.0	1.8	.4	-1.1	-2.5	-4.0	4.6	1.7	-1.3	-4.3	-7.3

	100 Hz					125 Hz				
INERTIA ERROR (%)	NATURAL FREQUENCY ERROR (%)					NATURAL FREQUENCY ERROR (%)				
	-1.0	-.5	0.0	.5	1.0	-1.0	-.5	0.0	.5	1.0
-1.0	-12.2	-6.1	0.0	6.1	12.3	-1.8	-.5	.7	2.0	3.2
-.5	-12.3	-6.2	0.0	6.2	12.4	-2.2	-.9	.4	1.6	2.9
0.0	-12.3	-6.2	0.0	6.2	12.4	-2.5	-1.3	0.0	1.3	2.6
.5	-12.4	-6.2	0.0	6.2	12.5	-2.9	-1.6	-.4	.9	2.2
1.0	-12.5	-6.2	0.0	6.3	12.5	-3.3	-2.0	-.7	.6	1.9

	150 Hz					175 Hz				
INERTIA ERROR (%)	NATURAL FREQUENCY ERROR (%)					NATURAL FREQUENCY ERROR (%)				
	-1.0	-.5	0.0	.5	1.0	-1.0	-.5	0.0	.5	1.0
-1.0	-.5	.2	.8	1.5	2.1	.0	.5	.9	1.3	1.7
-.5	-.9	-.2	.4	1.1	1.7	-.4	.0	.4	.9	1.3
0.0	-1.3	-.7	0.0	.7	1.3	-.8	-.4	0.0	.4	.9
.5	-1.7	-1.1	-.4	.3	.9	-1.3	-.9	-.4	-.0	.4
1.0	-2.1	-1.5	-.8	-.2	.5	-1.7	-1.3	-.9	-.4	-.0

The entire measurement system is under computer control. The details of the interactive program's logic is given in Appendix IV.

RESULTS

The apparatus and computer controlled test procedure were used to determine the complex shear modulus of an inhomogeneus polyurethane material with 4% of its volume containing air bubbles. The sample was 5.08 cm in diameter and its original height was 10.16 cm. Several different combinations of measurements were made to get an estimate of the variability of the complex shear modulus values as of function of slight changes in specimen temperature, choice of f_m and the height of the specimen. To determine the latter effect the original 10.16 cm high specimen was cut into two pieces, one 4.8 cm high and the other 4.9 cm high. The results are tabulated in Tables 5 and 6.

Comparing the results of the data in column 1 with those in column 2, 3 with 4, 5 with 6 and 7 with 8 in both tables it is seen that the repeatibility of the data is excellent; typically better than 1% for both the storage modulus and the loss tangent. Comparison of columns 3-6 of both tables indicates that the effect of a choice of f_m also yields a repeatibility of better than 1% for the storage modulus and 8% for the loss tangent. The large variation in the less tangent is consistent with the results implied by Tables 2-4.

Comparing columns 1 and 2 with columns 3 and 4 and with columns 7 and 8 it is seen that the change in length of the specimen yields results that are within 4% of each other. This small deviation is probably due to the unequal distribution of the air bubbles within the material.

Table 5

Variability of the Storage Modulus (G') as a Function of Several Test Parameters

	1	2	3	4	5	6	7	8	9
Length (cm)	10.16	10.16	4.8	4.8	4.8	4.8	4.9	4.9	4.9
f_m (Hz)	100.8	100.8	100.8	100.8	89.0	89.0	100.8	100.8	100.8
Temperature (°C)	24.0	24.2	21.2	21.9	23.2	23.2	21.1	22.3	22.6
Date	1 Sept 82	1 Sept 82	7 Sept 82	7 Sept 82	7 Sept 82	7 Sept 82	3 Sept 82	3 Sept 82	15 Sept 82
Time	11:39	12:18	9:36	10:27	14:52	15:49	9:29	11:09	15:11
Frequency (Hz)				G' (N/m^2)					
100			14.28	13.57	15.66	15.52			12.87
110	14.51	14.45	14.13	14.06	15.33	15.27	18.46	18.32	12.97
120	14.58	14.53	15.18	15.43	14.84	14.84	16.47	16.48	13.88
130	14.36	14.33	14.51	14.43	14.92	14.91	15.45	15.39	13.38
140	14.38	14.56	14.82	14.66	15.13	15.14	15.49	15.33	13.55
150	14.65	14.70	15.11	14.97	15.12	15.13	15.70	15.48	14.42
160	14.93	14.86	15.09	14.91	15.12	15.12	15.62	15.41	14.54
170	15.32	15.25	14.93	14.75	15.22	15.22	15.48	15.30	14.55
180	15.27	15.11	14.94	14.72	15.34	15.35	15.52	15.30	14.36
190	15.63	15.57	15.09	14.88	15.46	15.46	15.66	15.49	14.47
200	15.66	15.53	15.11	15.01	15.55	15.57	15.74	15.61	14.54
210			15.30	15.20	15.82	15.82	15.92	15.84	14.64
220			15.61	15.52	15.94	15.94	16.05	15.96	14.92
230			16.26	16.18	16.43	16.45	16.30	16.17	15.27
240			16.54	16.47	16.72	16.70	16.43	16.31	15.18
250			16.54	16.42	16.96	16.99	16.39	16.27	15.33
260			16.77	16.64	17.39	17.40	16.63	16.51	15.47
Test Site:	←			NBS			→		NSRDC

	1	2	3	4	5	6	7	8	9
Length (cm)	10.16	10.16	4.8	4.8	4.8	4.8	4.9	4.9	4.9
f_m (Hz)	100.8	100.8	100.8	100.8	89.0	89.0	100.8	100.8	100.8
Temperature (°C)	24.0	24.2	21.2	21.9	23.2	23.2	21.1	22.3	22.6
Date	1 Sept 82	1 Sept 82	7 Sept 82	7 Sept 82	7 Sept 82	7 Sept 82	3 Sept 82	3 Sept 82	15 Sept 82
Time	11:39	12:18	9:36	10:27	14:52	15:49	9:29	11:09	15:11
Frequency (Hz)				G"/G'					
100			.269	.173	.125	.140			.703
110	.224	.222	.360	.310	.184	.180	.238	.203	.406
120	.229	.227	.302	.249	.200	.204	.275	.269	.352
130	.230	.226	.250	.249	.210	.211	.231	.237	.320
140	.260	.287	.252	.250	.220	.220	.240	.238	.259
150	.255	.263	.254	.252	.218	.218	.247	.246	.226
160	.255	.256	.256	.253	.220	.220	.254	.252	.217
170	.241	.244	.253	.252	.210	.210	.246	.243	.222
180	.253	.223	.247	.249	.211	.211	.235	.230	.237
190	.224	.228	.260	.256	.215	.215	.237	.232	.240
200	.245	.248	.275	.271	.220	.218	.243	.241	.245
210			.287	.287	.232	.231	.241	.241	.249
220			.303	.302	.245	.245	.243	.240	.246
230			.291	.287	.245	.244	.242	.243	.249
240			.278	.275	.241	.243	.247	.248	.254
250			.280	.281	.238	.236	.251	.249	.253
260			.279	.278	.228	.226	.250	.250	.255
Test Site:	←			NBS			→		NSRDC

Comparing columns 7 and 8 with column 9 shows the change in values of the moduli due to the change in the test site. Although the loss tangent seem to remain unchanged the shear storage modulus inexplicably decreased by about 7%.

The apparatus and test method produce data that are self-consistent. In addition when the results are compared to values obtained previously from other tests at much higher frequencies, but on the same sample, these values are what are expected.

The 4.8 cm high specimen was tested over a range of temperatures from -10°C to 40°C with f_m = 100.8 Hz. The results are shown in Figures 7 and 8 where they exhibit the desired properties of high loss tangent at decreasing temperatures and of being relatively frequency independent. Unfortunately, from a rheological point of view this material does not exhibit the property of time-temperature equivalence and therefore cannot be reduced to a composite master curve that would effectively produce shear moduli data at a given temperture over a much greater frequency range than shown.

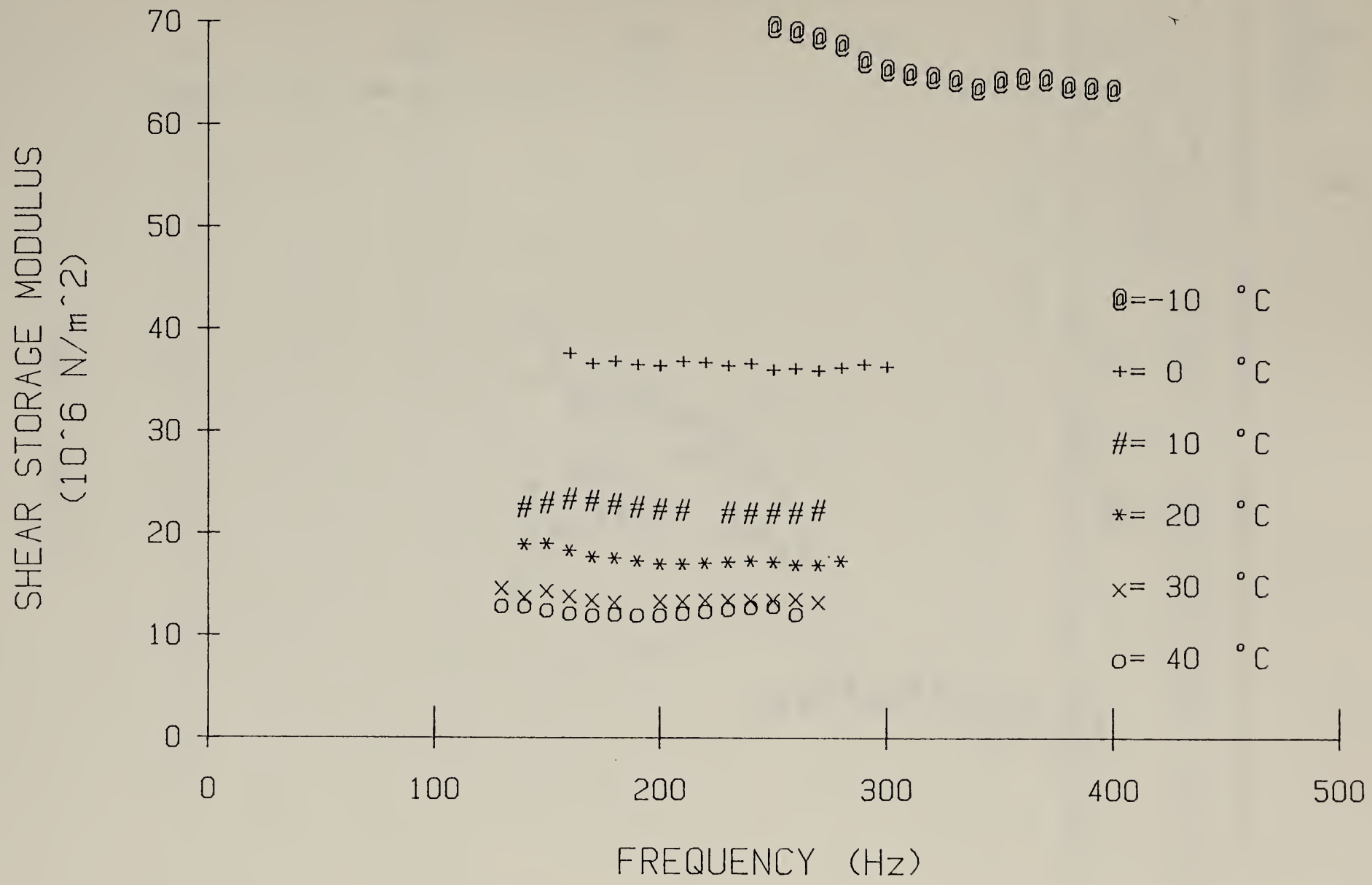

FIGURE 7 SHEAR STORAGE MODULUS OF POLYURETHANE WITH 4% AIR AS A FUNCTION OF FREQUENCY AND TEMPERATURE.

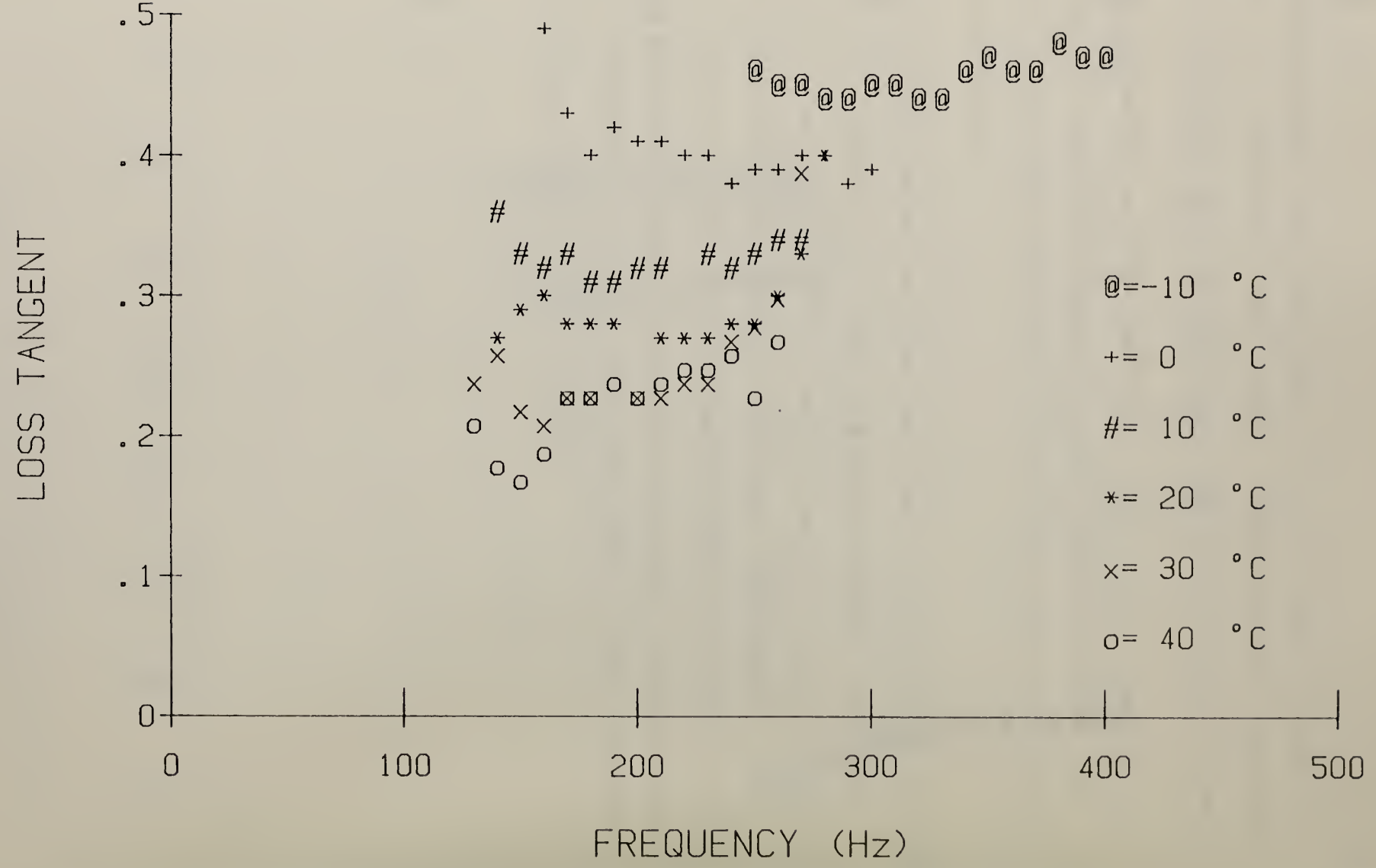

FIGURE 8 LOSS TANGENT OF POLYURETHANE WITH 4% AIR AS A FUNCTION OF FREQUENCY AND TEMPERATURE.

ACKNOWLEDGEMENT

The assistance of Mr. William Penzes, for his design and construction of the switching network, 30 dB amplifiers, and various power supplies and connectors, is gratefully acknowledged.

Mr. R. Reitz of the U.S. Naval Research and Development Center obtained the data presented in Figures 7 and 8.

REFERENCES

1) I. M. Ward, Mechanical Properties of Solid Polymers, John Wiley and Sons, London, (1971), Chapter 6.

2) L. Cremer, M. Heckl, and E. E. Unger, Structure-Borne Sound, Springer-Verlag, Berlin, (1973), pp 189-216.

3) "Measurement of Dynamic Moduli and Loss Factors of Visoelastic Materials," Session J, 99th Meeting: Acoustical Society of America, J. Acoust. Soc. of Amer., Suppl. 1, Vol. 67, Spring 1980, pp S23-S25.

4) W. J. Gottenberg and R. M. Christensen, "An Experiment for the Determination of the Mechanical Property in Shear for a Linear, Isotropic Viscoelastic Solid," Int. J. Engng. Sci., Vol. 2, (1964), pp 45-57.

5) J. H. Baltrukonis, D. S. Blomquist, and E. B. Magrab, "Measurement of the Complex Shear Modulus of a Linearly Visoelastic Material," Technical Report #5, Department of Engineering Mechanics, Catholic University of America, Washington, D. C. (May 1964).

6) D. W. Marquardt, "An Algorithm for Least Squares Estimation on Nonlinear Parameters," J. Soc. Ind. Appl. Math, Vol II (1963) pp 431-441.

7) J. C. Nash, Compact Numerical Methods for Computers: Linear Algebra and Function Minimization, John Wiley and Sons, New York, (1979), Chapter 17.

APPENDIX I

Marquardt's Minimization Procedure

The values of G' and G" are obtained from Eqs. (6) and (7) using Marquardt's methods [6, 7]. The method will be outlined below and the specific functions for our particular case will be given.

The Marquardt procedure is an efficient means of minimizing

$$S(\underset{\sim}{x}) = \sum_{i=1}^{m} [\underset{\sim}{f}_i(\underset{\sim}{x})]^2 = \underset{\sim}{f}^T \underset{\sim}{f} \tag{I-1}$$

where

$$f_i(\underset{\sim}{x}) = g_i(\underset{\sim}{x}) - g_i' \tag{I-2}$$

and $g_i(\underset{\sim}{x})$ are the m (nonlinear) functions of the parameters $\underset{\sim}{x}(x_1, x_2, ..x_n)$ and g_i' are the measured values. Equation (I-2) states that we are minimizing the sum of the squares of the deviation of the data from the functions used to fit these data. In our case, m = 2 and n = 2. The Marquardt procedure says that a good next guess for the value of the parameter $\underset{\sim}{x}$, denoted $\underset{\sim}{x} + \underset{\sim}{q}$, can be determined from an interactive solution to

$$(\underset{\sim}{J}^T \underset{\sim}{J} + \lambda \mathrm{Dia}[\underset{\sim}{J}^T \underset{\sim}{J}])\underset{\sim}{q} = -\underset{\sim}{J}^T \underset{\sim}{f} \tag{I-3}$$

where $\underset{\sim}{J}$ is the Jacobian matrix whose elements are defined as

$$J_{ij} = \frac{\partial}{\partial x_j} f_i(\underset{\sim}{x}) \tag{I-4}$$

The superscript T denotes the transpose of the matrix and Dia [...] denotes that the matrix has all zero elements except along its diagonal. The left hand side of Eq. (I-4) must be positive definite and, therefore, λ must always be chosen so that this side keeps its positive definiteness. The positive-definiteness is determined in the solution to Eq. (I-3) by using the Choleski decomposition of the matrix on the left hand side and checking to see that each diagonal term of the decomposed matrix is greater than zero, which indicates positive-definiteness. If they are not all greater than zero, the value of λ is increased by a factor of ten.

The interative solution itself is straightforward. Starting with a value of $\lambda = 0.1$, λ is reduced by a factor of 2.5 before each step in the solution if the preceding solution for $\underset{\sim}{q}$ has given

$$S(\underset{\sim}{x}+\underset{\sim}{q}) < S(\underset{\sim}{x})$$

If

$$S(\underset{\sim}{x}+\underset{\sim}{q}) \geq S(\underset{\sim}{x})$$

then λ is increased by a factor of 10. The process is repeated until certain convergence criteria have been satisfied.

For our particular case we have from Eqs. (6) that $x_1 = G'$, $x_2 = G''$, $g_1 = D'$, and $g_2 = \phi$, where, for convenience, we define $D' = (r_b/r_t)D$. Since D' and ϕ are functions of x and y, which in turn are functions of G" and G', it is easiest to use the chain rule for partial differentiation to obtain the four elements of the Jacobian matrix. Thus

$$J_{11} = \frac{\partial D'}{\partial G'} = \frac{\partial D'}{\partial x}\frac{\partial x}{\partial G'} + \frac{\partial D'}{\partial y}\frac{\partial y}{\partial G'}$$

$$J_{12} = \frac{\partial D'}{\partial G''} = \frac{\partial D'}{\partial x}\frac{\partial x}{\partial G''} + \frac{\partial D'}{\partial y}\frac{\partial y}{\partial G''}$$

$$J_{21} = \frac{\partial \phi}{\partial G'} = \frac{\partial \phi}{\partial x}\frac{\partial x}{\partial G'} + \frac{\partial \phi}{\partial y}\frac{\partial y}{\partial G'}$$

$$J_{22} = \frac{\partial \phi}{\partial G''} = \frac{\partial \phi}{\partial x}\frac{\partial x}{\partial G''} + \frac{\partial \phi}{\partial y}\frac{\partial y}{\partial G''}$$

where

$$\frac{\partial D'}{\partial x} = -[A^2 + B^2]^{-3/2}\left[A\frac{\partial A}{\partial X} + B\frac{\partial B}{\partial x}\right]$$

$$\frac{\partial D'}{\partial y} = -[A^2 + B^2]^{-3/2}\left[A\frac{\partial A}{\partial y} + B\frac{\partial B}{\partial y}\right]$$

$$\frac{\partial \phi}{\partial x} = [A^2 + B^2]^{-1}\left[A\frac{\partial B}{\partial x} - B\frac{\partial A}{\partial x}\right]$$

$$\frac{\partial \phi}{\partial y} = [A^2 + B^2]^{-1}\left[A\frac{\partial B}{\partial y} - B\frac{\partial A}{\partial y}\right]$$

A and B are given by Eq. (7) and their deviatives are

$$\frac{\partial A}{\partial x} = [(C_1 - 1)\sin(x) + C_1 x\cos(x)]\cosh(y) + C_1 y\sin(x)\sinh(y)$$

$$\frac{\partial A}{\partial y} = [C_1 x\sin(x) + (1 - C_1)\cos(x)]\sinh y - C_1\, y\, \cos(x)\, \cosh\, (y)$$

$$\frac{\partial B}{\partial x} = -\frac{\partial A}{\partial y}$$

$$\frac{\partial B}{\partial y} = [C_1 x\cos(x) + (C_1 - 1)\sin(x)]\cosh(y) + C_1 y\sin(x)\sinh(y)$$

The remaining partial derivatives are obtained from Eqs. (4). Thus,

$$\frac{\partial x}{\partial G'} = -\frac{1}{2p^2}\,[xG' - y\,G'']$$

$$\frac{\partial x}{\partial G''} = -\frac{1}{2p^2}\,[xG'' + y\,G']$$

$$\frac{\partial y}{\partial G'} = \frac{\partial x}{\partial G''}$$

$$\frac{\partial y}{\partial G''} = -\frac{\partial x}{\partial G'}$$

Returning to Eq. (I-3) we can now write the solution for q_1 and q_2 in terms of the elements of the Choleski decomposed matrix L_{ij} as

$$q_2 = v_1/L_{22}$$

$$q_1 = (v_1 - L_{21}\,q_2)/L_{11}$$

where

$$v_1 = b_1/L_{11}$$

$$v_2 = (b_2 - L_{21}v_1)/L_{22}$$

$$L_{11} = \sqrt{A_{11}}$$

$$L_{21} = A_{21}/\sqrt{A_{11}}$$

$$L_{22} = A_{22} - A_{21}^2/A_{11}$$

and

$$b_1 = J_{11}f_1 + J_{21}f_2$$

$$b_2 = J_{12}f_1 + J_{22}f_2$$

$$A_{11} = (1 + \lambda)\ (J_{11}^2 + J_{21}^2)$$

$$A_{12} = J_{11}J_{12} + J_{22}J_{21}$$

$$A_{22} = (1 + \lambda)\ (J_{12}^2 + J_{22}^2)$$

$$A_{21} = A_{12}$$

When $L_{22} > 0$ the matrix is positive definite.

APPENDIX II

Computation of the Mass Moment of Inertia J

The total mass moment of inertia, J, is comprised of the following parts: (1) the base of the torsion spring; (2) the accelerometer mounting arm, including the accelerometer and the counter balance; (3) the specimen mounting plate; and (4) the Allen screw heads. Referring to Figures A-1 to A-4, the following formulas and numerical values are obtained:

Torsion Spring Base

The mass moment of interia, J_D, using Figure A-1, is

$$J_2 = \frac{1}{2} W_D r_D^2$$

where, W_D is the weight of the base and is given by

$$W_D = \pi h_D r_D^2 \rho$$

where ρ is the density of the base material. For steel, $W_D = 0.09548$ kg and $J_D = 0.5825$ kg-cm^2.

Accelerometer Mounting Arm and Accelerometer

The mass moment of inertia, J_s, using Figure A-2 is

$$J_2 = \frac{W_c}{2}(r_o^2 + r_i^2) + 2W_o(\frac{L^2}{12} + d_2^2)$$

where

$$W_c = \rho h_A \pi (r_o^2 - r_i^2)$$

$$W_o = \rho h_A (LD - \pi r_A^2) + W_{ACC}$$

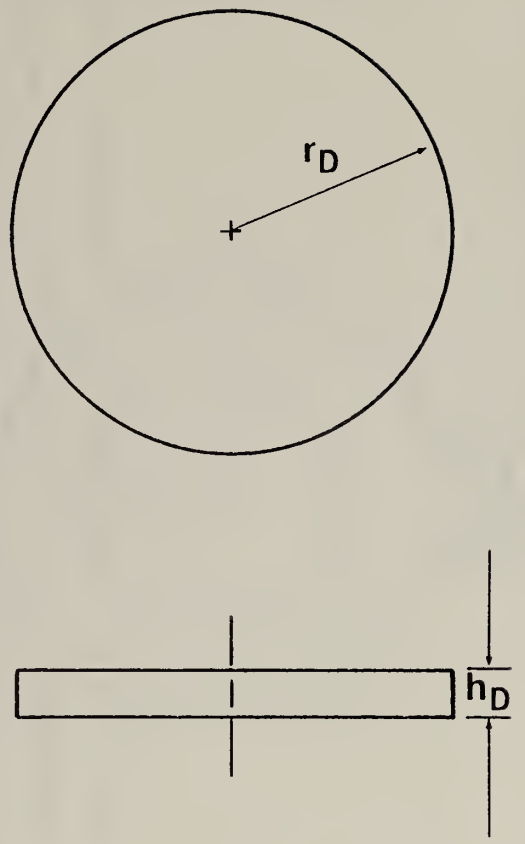

$r_D = 34.93\,mm$

$h_D = 3.18\,mm$

FIGURE A-1 DIMENSIONS OF TORSION SPRING BASE.

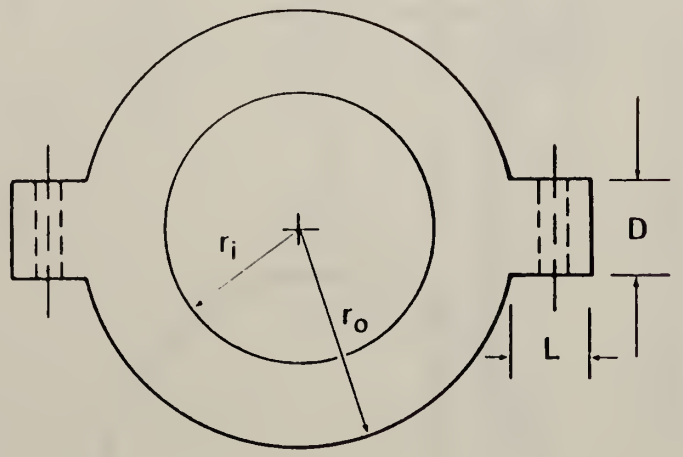

r_o = 34.93mm
r_i = 22.22mm
r_h = 2.54mm
d_1 = 47.63mm
d_2 = 41.28mm
D = 19.05mm
L = 12.7mm
h_A = 6.35 or 12.70mm

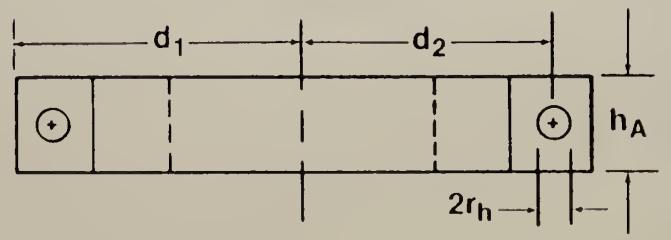

FIGURE A-2 DIMENSIONS OF ATTACHED MASS AND TOP ACCELEROMETER'S MOUNTING POSITION.

and W_{ACC} is the weight of the accelerometer (2.5 gm). For aluminum, W_C = $(6.190 \times 10^{-3})h_A$ kg and $W_o = (6.013 \times 10^{-4})h_A + 0.0025$ kg. Then for h_A = 6.35 mm, $J_S = 0.4680$ kg-cm^2 and for h_A = 12.7 mm, $J_S = 0.9360$ kg-cm^2.

Specimen Mounting Plate

The mass moment of inertia, J_M, using Figure A-3, is

$$J_M = \frac{1}{2}(W_t r_t^2 + W_b r_b^2)$$

where

$$W_t = \rho h_t \pi r_t^2$$

and

$$W_b = \rho h_b \pi r_b^2$$

For aluminum, $W_t = 0.03307$ kg and $W_b = 0.05355$ kg. The $J_M = 0.7308$ kg-cm^2.

Allen Screw Heads

The mass moment of inertia, J_H, using Figure A-4, is,

$$J_H = 4[W_b(\frac{1}{2}r_c^2 + d_3^2) + W_t(\frac{1}{2}(r_c^2 + r_d^2) + d_3^2)]$$

where

$$W_b = \rho h \pi r_c^2$$

and

$$W_t = \rho h\ \pi(r_c^2 - r_d^2)$$

For the large screws, $W_b = 0.00149$ kg and $W_t = 0.00105$ kg. For the small screw, $W_b = 0.000621$ kg and $W_t = 0.000345$ kg. Then, for the large screws $J_H = 0.08408$ kg-cm^2 and for the small screws $J_H = 0.03185$ kg-cm^2. The total is $J_H = 0.1159$ kg-cm^2.

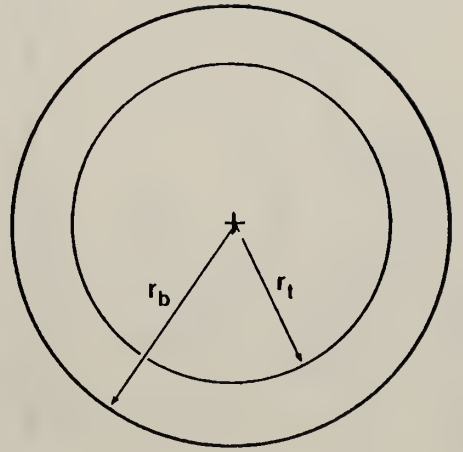

r_b = 44.45mm

r_t = 34.93mm

h_t = 3.18mm

h_B = 3.18mm

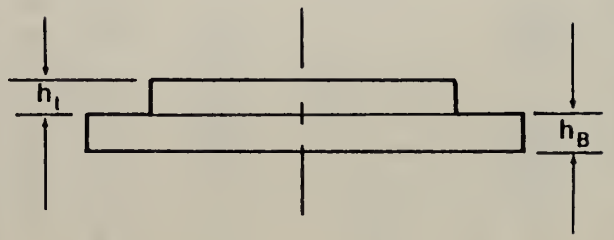

FIGURE A-3 DIMENSIONS OF SPECIMEN MOUNTING PLATE.

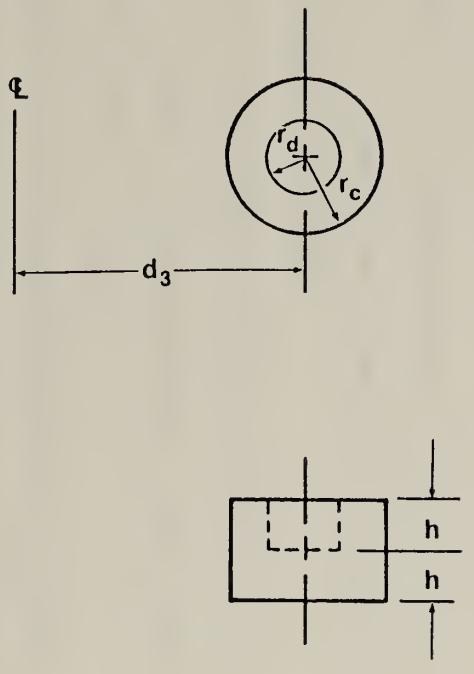

	LARGE	SMALL
h	3.18mm	1.98mm
r_d	2.38mm	2.38mm
r_c	4.37mm	3.57mm
d_3	28.58mm	

FIGURE A-4 DIMENSIONS OF ALLEN SCREW HEADS.

Total Mass Moment of Inertia

The mass moment of inertia is equal to

$$J = J_D + J_S + J_M + J_H$$

For the two accelerometer mounting plates of thickness h_A we have:

h_A = 6.35 mm: $J = 1.8972$ kg-cm^2

h_A = 12.7 mm: $J = 2.3652$ kg-cm^2

APPENDIX III

Computer-Controlled Relay Switches

The schematic diagram of the switching functions and connection to the computer-controlled switching box is shown in Figure 4. The BNC connectors to the switching box are depicted as two concentric circles in the figure and the label that appears next to the BNC connector on the relay switching box is also given in the figure. Each of the relays is controlled by one of the 16 lines available on the output of the HP 98032A 16-bit interface, which is connected from the computer to the switching box.

Following the nomenclature of the 16-bit interface manual, the lines denoted D0XX are connected as follows:

D00 Sets attenuator to 5 dB

D01 Sets attenuator to 10 dB

D02 Sets attenuator to 15 dB

D03 Sets attenuator to 20 dB

D04 Sets attenuator to 25 dB

D05 Sets attenuator to 30 dB

D06 Connects accelerometer #2 to fixed gain amplifier of channel #2 when external switch is in test position, otherwise it connects directly to phasemeter and the digital voltmeter.

D07 Connects oscillator to fixed gain amplifier of channel #2 when D015 is 'low' or connects the output of the attenuator to the fixed gain amplifier of channel #2 when D015 is 'high'.

D08 Connects accelerometer #1 to fixed gain amplifier of channel #1 when external switch is in test position, otherwise it connects directly to phasemeter and the digital voltmeter.

D09 Connects oscillator to fixed gain amplifier of channel #1 when D015 is 'low' or connects the output of the attenuator to the fixed gain amplifier of channel #1 when D015 is 'high'.

D010 Connects accelerometer #1 or tracking filter output of channel #1 to the digital voltmeter.

D011 Connects accelerometer #2 or tracking filter output of channel #2 to the digital voltmeter.

D012 Connects oscillator output to the digital voltmeter.

D013 Connects oscillator output to the amplifier.

D014 Sets attenuator to 0 dB.

D015 Reverse D07 and D09: Connects D07 to attenuator output and D09 to the oscillator output.

If N is an integer value of a 16-bit binary number that activates the appropriate lines to control the relays and XX in the denotation DOXX indicates the N-1 bit location of the 16-bit binary number, then the following list shows the correspondence between N and the lines set "high." (See the main text for a discussion of the test protocols used.) As a last remark it is mentioned that the attenuator's impedance is such that it loads the oscillator's output to a value that is approximately 6 dB less than if the oscillator were to be connected to a high impedance device. This fact is taken into account in subroutine 'Instr' (see Appendix IV).

N	Lines 'High' (switch closed)
9536	D06, D08, D010, D013
10560	D06, D08, D011, D013
4096	D012

9216	D010, D013 (for back-to-back accelerometer calibration only)
10240	D011, D013 (for back-to-back accelerometer calibration only)
1664+M+S	D07, D09, D010, see below
2688+M+S	D07, D09, D011, see below

where

M	Lines 'High' (switch closed)
16384	D014
1	D00
2	D01
4	D02
8	D03
16	D04
32	D05

and

S	
0	---
-32768	D015

In Figure 4 the relay symbols have their corresponding D0XX value adjacent to them. The two pairs of relays (D06, D07) and (D08, D09) and the triplet of relays (D010, D011, D012) are each connected such that only one of each pair or triplet of relays can be closed at a time.

APPENDIX IV

Subroutine Names and Their Functions

Accplo - Plots measured acceleration levels versus frequency.

DVM - Controls and reads the Ballantine digital voltmeter.

Freqax - Draws 'tic'-marks and labels the logrithmic frequency axis.

Freqmn - Determines upper and lower limits of the plotted frequency axis based on the minimum and maximum test frequencies selected.

Freqsel - Queries user for starting and ending test frequencies and calculates all test frequencies in between these limits.

Graph - Plots experimentally determined acceleration levels and phase angles as a function of frequency. [Calls Subr. - Accplo, Freqax, Freqmn, Header, Phaplt, Phasis, Vertax, Vrange].

Guess - Before entering subroutine 'Mark' for the first time it completes an initial estimate of G' and G" from the measured acceleration ratio corresponding to the lowest frequency. The phase angle is set equal to zero.

Header - Prints headings containing all pertinent test data prior to printing all tabulated and graphical output.

Instr - Runs the complete measurement protocal for either experiment: back-to-back calibration of accelerometers or determination of shear modulus. [Calls Subr. - Dvm, Osc, Pmeter, Switch.]

Mark - Performs nonlinear least squares fit to each pair of acceleration ratio and phase angle at a given frequency. Special subroutine 'Ftn' is part of this subroutine to speedup the computation process. [Calls Local Subr. - 'Ftn'.]

Osc - Sets frequency and amplitude of Rockland frequency synthesizer.

Para - Queries user for all pertinent test parameters prior to the start of the test.

Phaplt - Plots the measured phase angles as a function of frequency.

Phaxis - Draws 'tic'-marks and labels the vertical axis for measured phase data.

Pmeter - Controls and reads the Dranetz phasemeter.

Scan - Measures only the acceleration ratio over any frequency range, frequency increment and excitation amplitude. [Calls Subr - Dvm, Osc, Switch.]

Switch - Controls sixteen relay switches to perform the various measurement protocals and directs the accelerometer signals to the digital voltmeter and phasemeter.

Table - Tabulates all experimetally obtained and calculated results. [Calls Subr - Header.]

Vertax - Draws 'tic'-marks and labels the vertical axis for measured acceleration levels.

Vrange - Determines the upper and lower amplitude limits for the acceleration level plot.

APPENDIX V

Program Flow Chart
Main Program: "SHRMOD"

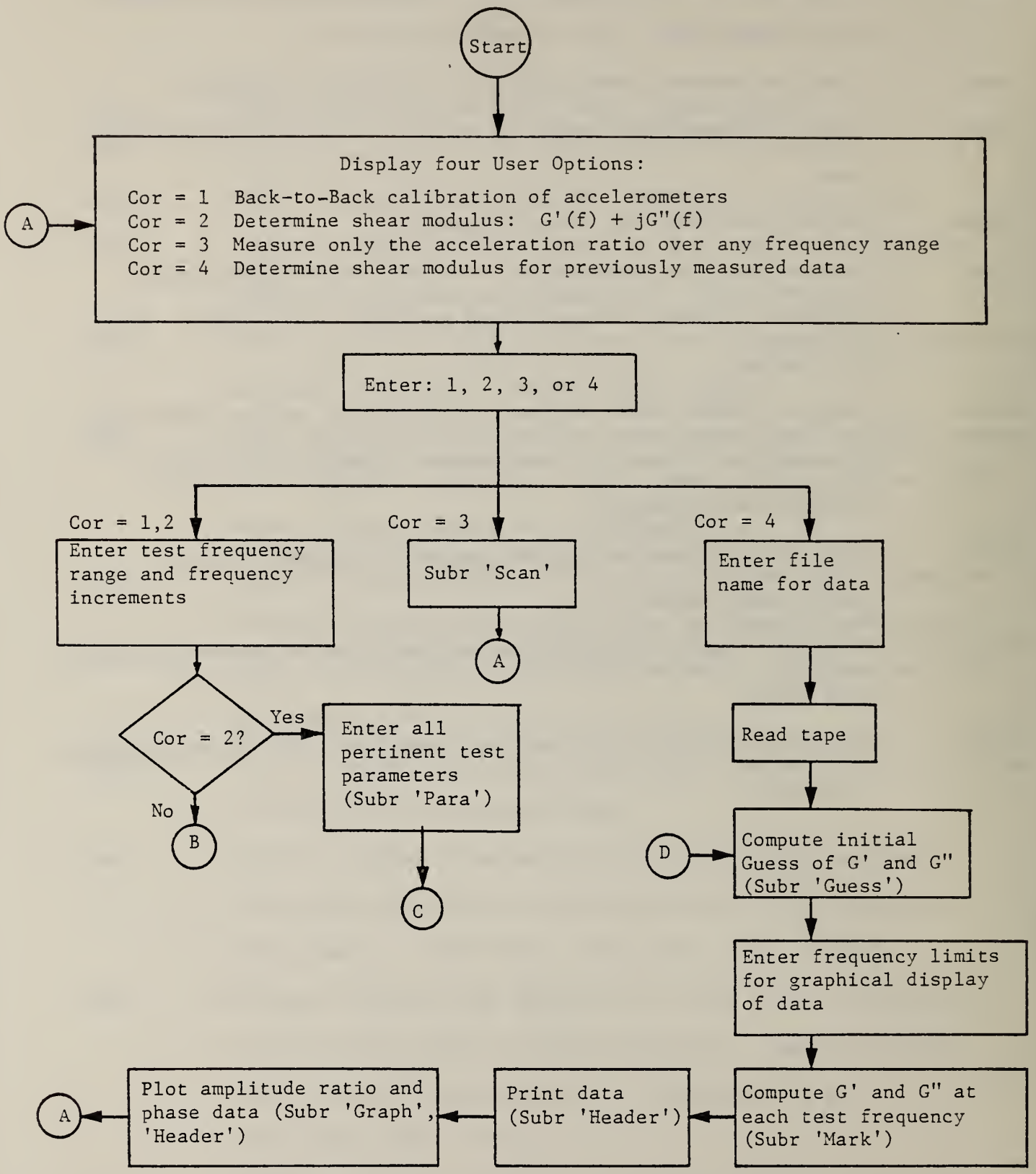

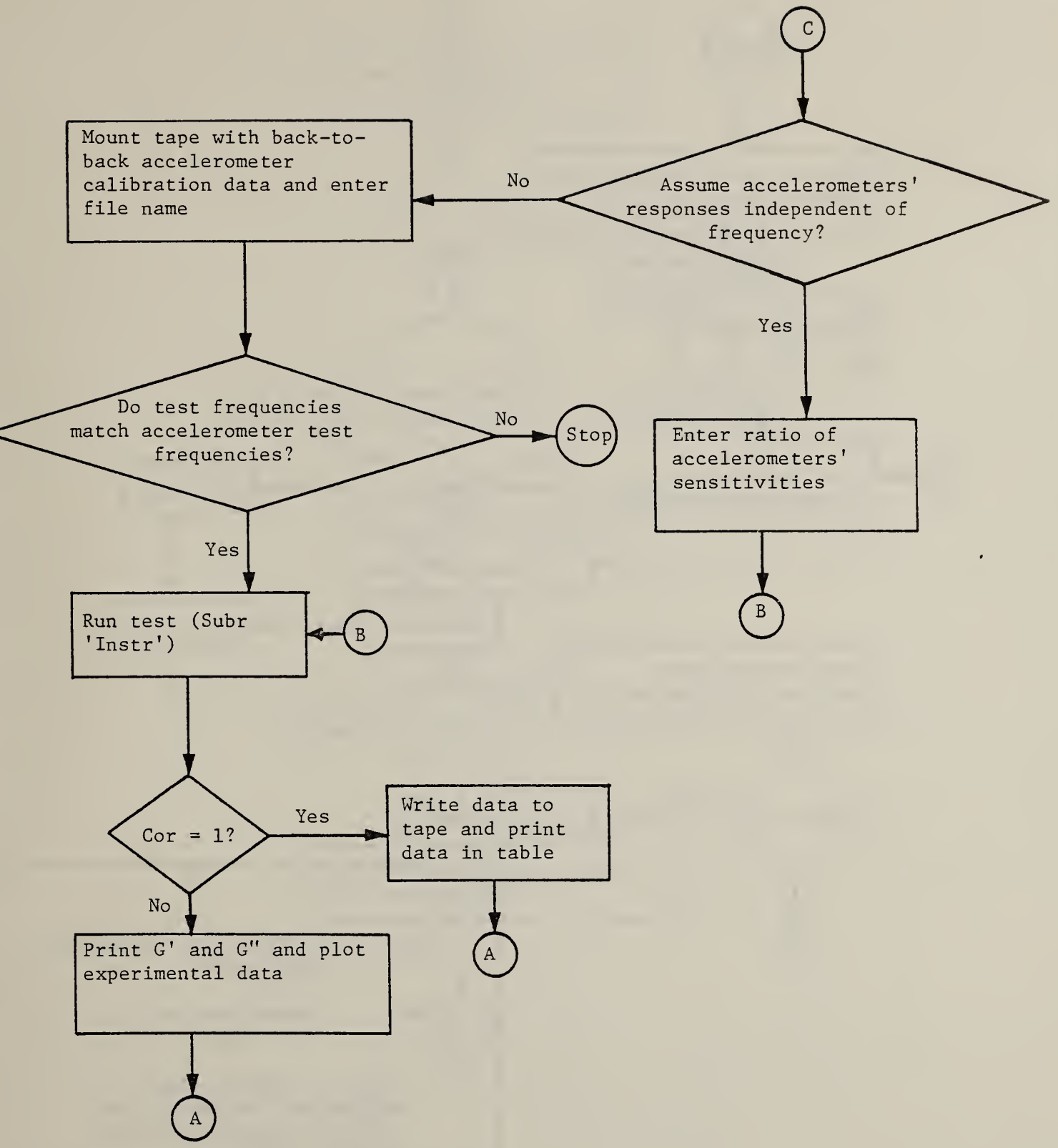
C
Assume accelerometers' responses independent of frequency?
No
Mount tape with back-to-back accelerometer calibration data and enter file name
Yes
Enter ratio of accelerometers' sensitivities
B
Do test frequencies match accelerometer test frequencies?
No
Stop
Yes
Run test (Subr 'Instr')
B
Cor = 1?
Yes
Write data to tape and print data in table
A
No
Print G' and G" and plot experimental data
A

Subroutine: 'Instr'

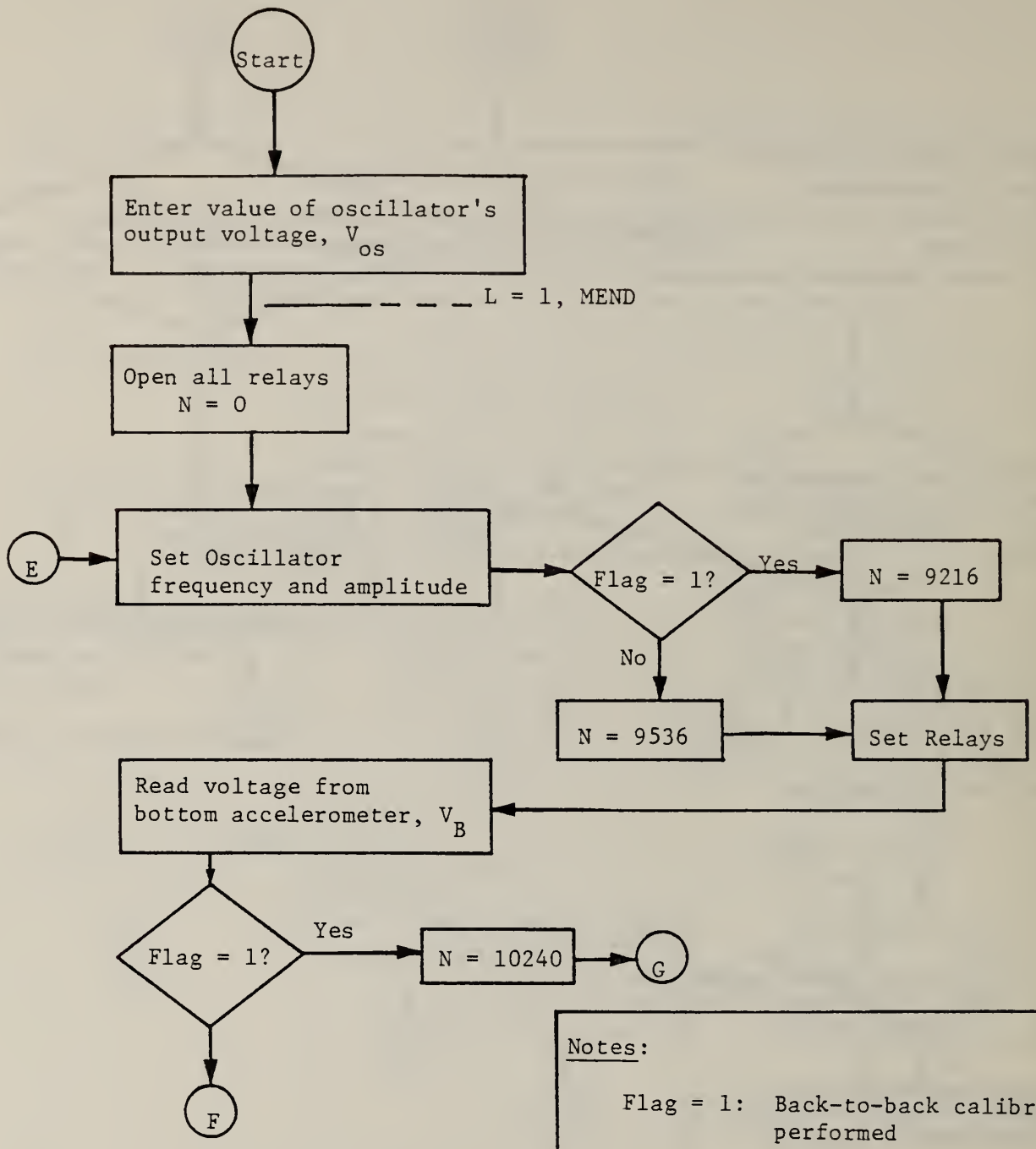

Notes:

Flag = 1: Back-to-back calibration performed

Flag = 2: Shear modulus test performed

N: Value of integer used by subroutine "Switch" to set relays in switch box (see Appendix III)

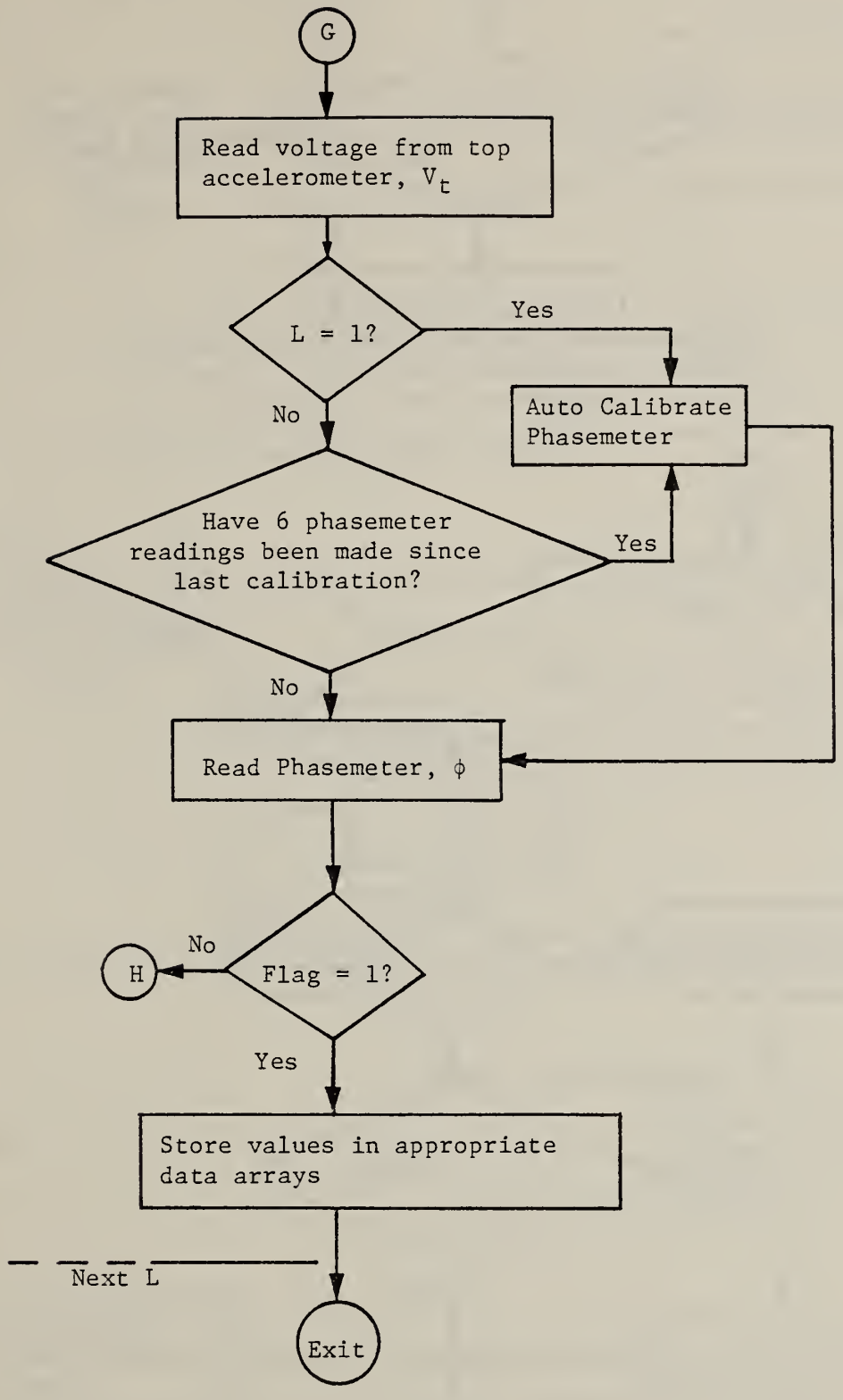
G
Read voltage from top accelerometer, V_t
L = 1?
Yes
No
Auto Calibrate Phasemeter
Have 6 phasemeter readings been made since last calibration?
Yes
No
Read Phasemeter, ϕ
No
H
Flag = 1?
Yes
Store values in appropriate data arrays
Next L
Exit

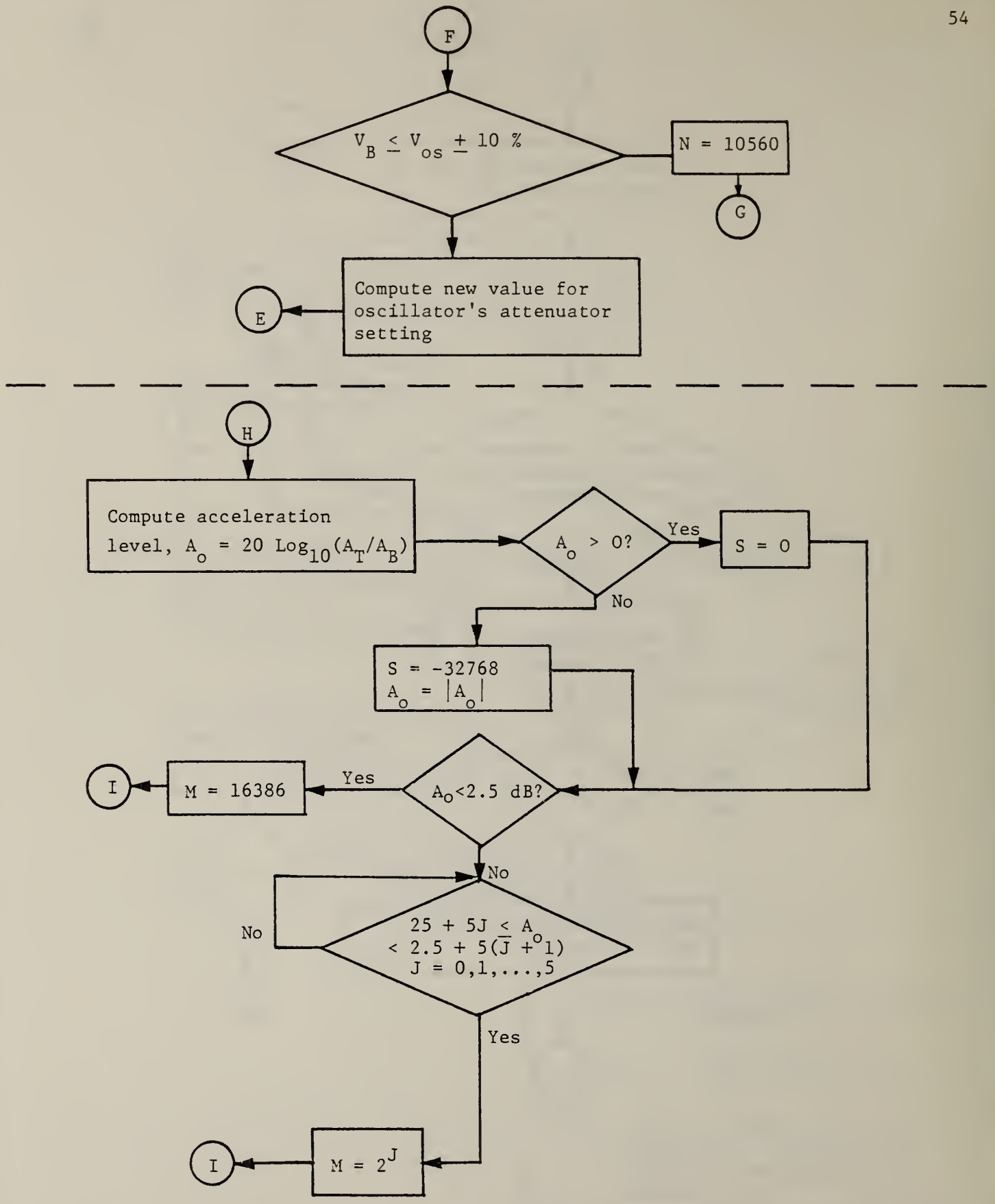
F
$V_B \leq V_{os} \pm 10\ \%$
N = 10560
G
Compute new value for oscillator's attenuator setting
E
H
Compute acceleration level, $A_o = 20\ Log_{10}(A_T/A_B)$
$A_o > 0$?
Yes
S = 0
No
S = -32768
$A_o = |A_o|$
A_o<2.5 dB?
Yes
M = 16386
I
No
$25 + 5J \leq A_o < 2.5 + 5(J+1)$
$J = 0,1,\ldots,5$
No
Yes
$M = 2^J$
I

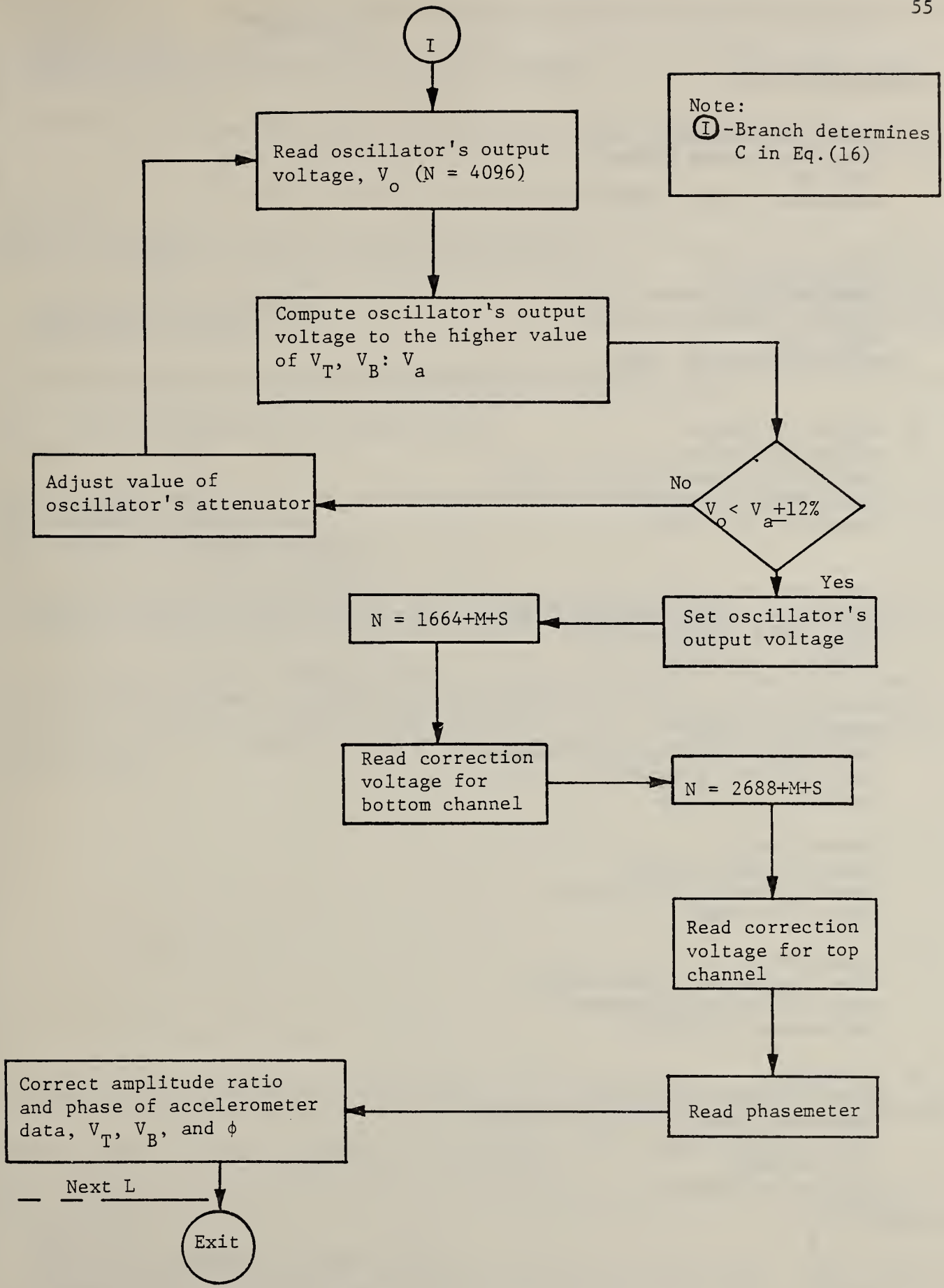
I
Note:
(I)-Branch determines C in Eq.(16)
Read oscillator's output voltage, V_o (N = 4096)
Compute oscillator's output voltage to the higher value of V_T, V_B: V_a
Adjust value of oscillator's attenuator
No
$V_o < V_a \pm 12\%$
Yes
N = 1664+M+S
Set oscillator's output voltage
Read correction voltage for bottom channel
N = 2688+M+S
Read correction voltage for top channel
Correct amplitude ratio and phase of accelerometer data, V_T, V_B, and ϕ
Read phasemeter
Next L
Exit

DISTRIBUTION LIST

1) Commander (2 copies)
Naval Sea Systems Command
Code 55N
Washington, D. C. 20362

2) Commander
Naval Surface Weapons Center
Code R31 (Walter Madigosky)
White Oak
Silver Spring, Md 20910

3) Officer in Charge
Annapolis Laboratory
David Taylor Naval Ship R&D Center
Code 2842 (John Eynck)
Annapolis, Md 21402

4) Commander (6 copies)
David Taylor Naval Ship R&D Center
Code 1905.2 (Wayne Reader)
Bethesda, Md 20084

5) Commander (1 copy)
David Taylor Naval Ship R&D Center
Code 1965 (Bruce Douglas)
Bethesda, Md 20084

6) Edward Hobaica
Electric Boat Division
General Dynamics Corporation
Groton, CN 06340

7) Commander
Naval Underwater Systems Center
Code 3392 (Charlie Sherman)
New London, CT 06320

8) Commander
Naval Research Laboratory
Underwater Sound Reference Division
Attn: Robert Ting
P.O. Box 8337
Orlando, FL 32856

NBS-114A (REV. 2-8C)

U.S. DEPT. OF COMM. BIBLIOGRAPHIC DATA SHEET (See instructions)	1. PUBLICATION OR REPORT NO.	2. Performing Organ. Report No.	3. Publication Date
	NBSIR 83-2776	738.00	September 1983

4. TITLE AND SUBTITLE

Determination of the Viscoelastic Shear Modulus Using Forced Torsional Vibrations

5. AUTHOR(S)

Edward B. Magrab

6. PERFORMING ORGANIZATION (If joint or other than NBS, see instructions)

NATIONAL BUREAU OF STANDARDS
DEPARTMENT OF COMMERCE
WASHINGTON, D.C. 20234

7. Contract/Grant No.

N00024FQ02013 (NavSea 05E)

8. Type of Report & Period Covered

Final 1980-1982

9. SPONSORING ORGANIZATION NAME AND COMPLETE ADDRESS (Street, City, State, ZIP)

U.S. Naval Ship Research Development Center
Bethesda, Md 20084

10. SUPPLEMENTARY NOTES

N00024RQ02013 (NavSea 05H)
MIRP N00167-81-MP-00009 (DTNSRDC)
MIRP N00167-82-WR2-0504 (DTNSRDC)

☐ Document describes a computer program; SF-185, FIPS Software Summary, is attached.

11. ABSTRACT (A 200-word or less factual summary of most significant information. If document includes a significant bibliography or literature survey, mention it here)

A forced torsional vibration system has been developed to measure the shear storage and loss moduli on right circular cylindrical specimens whose diameter can vary to 9 cm and whose length can vary from 2 to 15 cm. The method and apparatus are usable over the frequency range 80 to 550 Hz and a temperature range of -20°C to 80°C.

12. KEY WORDS (Six to twelve entries; alphabetical order; capitalize only proper names; and separate key words by semicolons)

shear modulus; torsion; vibrations; viscoelastic

13. AVAILABILITY

☒ Unlimited

☐ For Official Distribution. Do Not Release to NTIS

☐ Order From Superintendent of Documents, U.S. Government Printing Office, Washington, D.C. 20402.

☒ Order From National Technical Information Service (NTIS), Springfield, VA. 22161

14. NO. OF PRINTED PAGES

61

15. Price

$10.00

USCOMM-DC 6043-P80